ADVANCES IN INORGANIC CHEMISTRY, VOL. 41

INTERVALENCE CHARGE TRANSFER AND ELECTRON EXCHANGE STUDIES OF DINUCLEAR RUTHENIUM COMPLEXES

ROBERT J. CRUTCHLEY

The Ottawa–Carleton Chemistry Institute, Carleton University, 1125 Colonel By Dr., Ottawa, Ontario, K1S 5B6, Canada

I. Introduction

Dinuclear ruthenium complexes form the largest group by far of any mixed-valence system and are the exclusive subject of this chapter. Ruthenium is the transition metal of choice to study electron transfer or exchange because it is relatively inexpensive and forms stable Ru(III) and Ru(II) coordination complexes. In addition, the synthetic coordination chemistry of ruthenium is well developed (*1*).

The intellectual push to study mixed-valence complexes was provided by the publication in 1967 of two review articles, by Allen and Hush (*2*) and Robin and Day (*3*), on the physical properties of mixed-valence systems. These were followed by Hush's publication (*4*) of his theoretical model of intervalence transitions, which provided a link between the properties of mixed-valence complexes in solution and the Marcus theory of intermolecular electron transfer (*5, 6*). The review by Robin and Day classified mixed-valence complexes into three types: class I,

Copyright © 1994 by Academic Press, Inc.
All rights of reproduction in any form reserved.

completely valence trapped (no coupling between metal ions); class II, valence trapped (weak coupling between metal ions); and class III, delocalized valency (strong coupling between metal ions). These ideas, complete with comparisons of mixed-valence complex properties with Marcus electron transfer theory, formed the basis of Creutz's review of mixed-valence complexes in 1983 (*7*).

Since the publication of Creutz's review, many new complexes have been synthesized and important developments have occurred. This chapter surveys the literature from 1982 to August of 1993, and it is meant to be an extension of the Creutz review and a guide to the experimentalist in the design of novel dinuclear ruthenium complexes for the study of superexchange phenomena.

The reader should be familiar with the above reviews, and it would be useful to have a basic understanding of excited-state (*8*) and thermal (*9*) electron transfer. A quantum mechanical approach to these subjects can be found in a recent review by Newton (*10*).

This chapter is broken up into two main sections: mixed-valence complexes and electron exchange. The section on mixed-valence complexes discusses the various theoretical approaches with a strong emphasis on the Hush model, a summary of new class III complexes, and a summary of class II complexes. The section on electron exchange begins with an introduction to magnetic exchange theory, in which a charge-transfer model for superexchange is discussed, and ends with a discussion of dinuclear ruthenium complexes that undergo antiferromagnetic spin coupling. The section on future studies summarizes important developments and research that is needed to increase understanding of superexchange phenomena. The practical applications of this research to molecular devices and materials is also pointed out. Finally a glossary of abbreviations and organic ligand structures is included at the end of the review.

II. Mixed-Valence Complexes

A. The Theory of Mixed-Valence Systems

1. The Hush Model

The conceptual framework that is used to understand thermal and photoinduced electron transfer is illustrated by a classical potential energy-configuration diagram. The simpliest case for electron transfer in which the electron is coupled between donor and acceptor by a single oscillator having the same frequency in both the initial and the final states is illustrated in Figs. 1a and 1b.

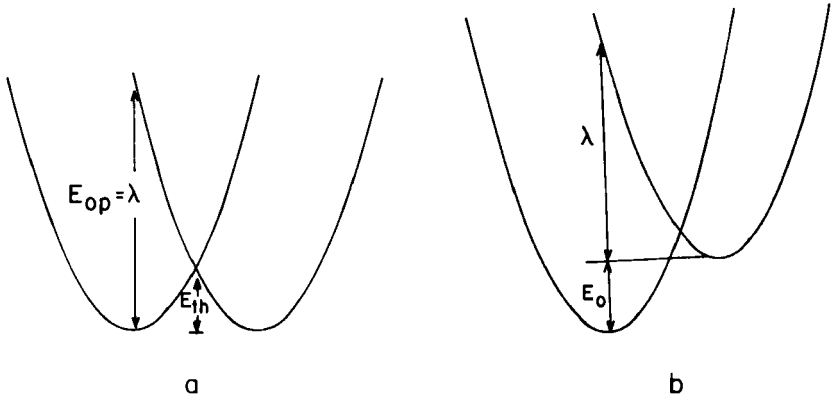

FIG. 1. Potential energy-configuration diagram of initial and final states for (a) symmetric mixed valence complex and (b) asymmetric mixed valence system.

For Figs. 1a (symmetric case) and 1b (asymmetric case), the left-hand curve is that for the initial state and the right-hand curve, that for the final state. For the symmetric case there is no energy difference between the initial and the final states ($E_0 = 0$) but for the asymmetric case $E_0 > 0$. The vertical transition between initial and final states (E_{op}) is the energy required to photoexcite an electron between states. This is the intervalence transition (IT) or, in the case of the dinuclear ruthenium complexes of this chapter, metal-to-metal charge transfer (MMCT). A thermal electron transfer route arises from the vibronic coupling of initial and final states and has the activation energy E_{th}. When donor and acceptor interact, initial and final states mix and this causes a distortion in the potential energy curve (Fig. 2). The thermal activation energy E_{th} becomes smaller with increasing magnitude of the resonance exchange integral H_{ad}. The Marcus theory of bimolecular electron transfer rates (*5, 6*) used the above conceptual framework to

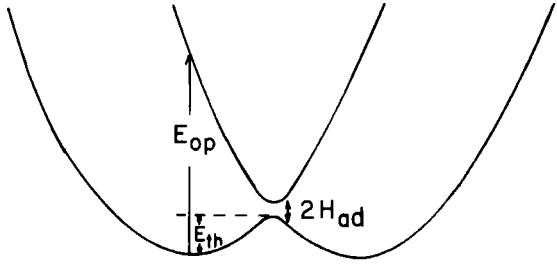

FIG. 2. Distortion of potential energy curves resulting from mixing of initial and final states.

understand the dependence of E_{th} on the nature of weakly coupled donor and acceptor complexes. It was Hush (*4*) who applied this conceptual framework to the problem of intervalence transitions.

For the weak coupling case (class II complexes), in which the distortion seen in Fig. 2 is small, Hush derived the following relationships of intervalence band properties: For the symmetric system (Fig. 1a),

$$E_{op} = 4E_{th}, \tag{1}$$

$$\Delta\nu_{1/2} = (2310\nu_{max})^{1/2}. \tag{2}$$

For the asymmetric system (Fig. 1b),

$$E_{op} = \lambda + E_0, \tag{3}$$

$$\Delta\bar{\nu}_{1/2} = [2300(\nu_{max} - E_0)]^{1/2}. \tag{4}$$

The band width at half peak height $\Delta\bar{\nu}_{1/2}$ assumes a Gaussian band shape and is in cm^{-1}. $\Delta\bar{\nu}_{1/2}$ is defined as the value of $\Delta\bar{\nu}$ at which

$$\frac{I_v\bar{\nu}_{max}}{I_{max}\bar{\nu}} = \frac{1}{2} \tag{5}$$

but that it is most commonly evaluated as $\Delta\bar{\nu}$, for which $I/I_{max} = \frac{1}{2}$.

For weak coupling cases, Hush showed that the intensity of an intervalence transition was related to the extent of coupling between donor and acceptor. The derivation (*11*) begins by considering the theoretical expression for oscillator strength,

$$f = 1.085 \times 10^{11} G\bar{\nu}_{max} D, \tag{6}$$

where G refers to the degeneracy of the states concerned, $\bar{\nu}_{max}$ is approximated to be the energy of the intervalence band in cm^{-1} at maximum extinction coefficient ε_{max}, and D is the dipole strength for an electric-dipole-allowed transition. For a one-electron system, D is related to the charge-transfer transition dipole moment M, by

$$M = \langle\psi_g|er|\psi_e\rangle = eD^{1/2}, \tag{7}$$

where ψ_g is the ground-state wave function, ψ_e is the excited-state wave function, and er is the transition dipole operator. The square of the electric charge, e^2, is usually incorporated into the prefactor of Eq. (6). Hush considered isolated donor ϕ_d and acceptor ϕ_a wave functions to

be weakly coupled and, following Murrell (*12*), the resulting ground- and excited-state wave functions can be written

$$\psi_g = \phi_d + \alpha_{ad}\phi_a \tag{8}$$

$$\psi_e = \phi_a + \alpha_{da}\phi_d. \tag{9}$$

These wave functions are orthogonal and so

$$\alpha_{ad} + \alpha_{da} + S_{ad} = 0, \tag{10}$$

where S_{ad} is the overlap integral between donor and acceptor wave functions. For the weak coupling case, $S_{ad} \simeq 0$ and the mixing coefficients $\alpha_{ad} = -\alpha_{da} = \alpha$. Then by perturbation theory

$$\alpha = H_{ad}/E_d - E_a \approx H_{ad}/\bar{\nu}_{max}, \tag{11}$$

where H_{ad} is the resonance exchange integral in cm^{-1}, which is a measure of electronic coupling, and $E_d - E_a$ is the difference in energy in cm^{-1} between donor and acceptor wave functions, which can be approximated by $\bar{\nu}_{max}$.

Substituting Eqs. (8) and (9) into Eq. (7) yields after simplification (*13*),

$$M \cong \alpha eR, \tag{12}$$

where R is the transition dipole length (the distance through which charge is carried) in centimeters. Equations (11) and (12) can be used to solve for dipole strength in Eq. (7) and the result substituted into Eq. (6) yields

$$f = 1.085 \times 10^{11} G H_{ad}^2 R^2/\bar{\nu}_{max}. \tag{13}$$

The oscillator strength of a Gaussian band can be determined experimentally (*11*) by using the expression

$$f = 4.6 \times 10^{-9} \varepsilon_{max} \bar{\nu}_{1/2}. \tag{14}$$

Substituting Eq. (14) for f and rearranging gives

$$H_{ad} = \frac{2.06 \times 10^{-2}}{R} \cdot (\bar{\nu}_{max} \cdot \varepsilon_{max} \cdot \bar{\nu}_{1/2})^{1/2}. \tag{15}$$

The Hush model allows the experimentor to estimate the amount of metal–metal coupling (H_{ad} and α) provided an intervalence band is experimentally observable and R can be estimated.

In the case of strong coupling (class III complexes), for which it is no longer appropriate to use perturbation theory, the interaction of states is so great that bonding and antibonding potential energy curves result (the potential energy diagram for a symmetric mixed valence complex is shown in Fig. 3). The magnitude of H_{ad} has become so great that $E_{th} = 0$. The odd electron can now move freely between metal centers (delocalized) and the energy of the intervalence transition is a measure of electronic coupling between donor and acceptor wave functions,

$$E_{op} = 2H_{ad}. \tag{16}$$

Because the ground state is delocalized between metal ions, it is not strictly appropriate to describe the intervalence transition band of a class III complex as a metal-to-metal charge transfer transition. Nevertheless, the MMCT designation will be used for the sake of simplicity.

The dependence of intervalence transition energy on the activation barrier to thermal electron transfer in Eqs. (1) and (3) allows the solvent dependence of intervalence transitions to be understood in terms of relationships developed for the Marcus Theory of electron transfer (*5, 6*).

For a weakly coupled symmetric system, E_{op} can be written (*4*) approximately as

$$E_{op} = \chi_i + \chi_o + \Delta E', \tag{17}$$

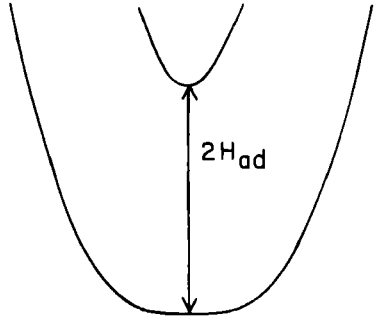

FIG. 3. Potential energy diagram for a symmetric class III mixed valence complex.

where $\Delta E'$ accounts for any additional energy associated with excitation to either a spin-orbit or a ligand-field excited state (*14–16*), χ_i is the inner sphere reorganization parameter, which can be written,

$$\chi_i = \frac{n(2f_2f_3)(d_2 - d_3)}{f_2 + f_3}, \tag{18}$$

and χ_0 is the outer sphere reorganization parameter, which can be expressed in the form,

$$\chi_o = e^2(1/r - 1/d)(1/D_{op} - 1/D_s), \tag{19}$$

where d_2,d_3 and f_2,f_3 are the metal–ligand bond lengths and the force constants for the metals in oxidation states II and III, respectively, r is the molecular trapping site radius, d is the distance between metal centers, and D_{op} and D_s are the optical and static dielectric constants of the sovlents.

From Eq. (19), E_{op} should be linearly proportional to the solvent term $(1/D_{op} - 1/D_s)$. This relationship has been demonstrated for weakly coupled mixed valence complexes (see Section (II.C.2.c) and this gives qualitative support to the Hush model.

The recent application of electroabsorption (Stark effect) spectroscopy to mixed valence complexes has shown that the actual charge transfer distance [R in Eq. (15)] is considerably smaller than the metal-to-metal separation (*17, 18*). This was not unexpected because it has been previously suggested (*7*) that the donor or acceptor wave function can extend itself onto the LUMO or HOMO of the bridging ligand, respectively. A consequence of this is that values of H_{ad} derived using Eq. (15) are significantly underestimated in the Creutz review (*7*) and Table VI of this chapter, which used metal–metal separation for R. In addition, the larger molecular trapping radius r means that a key boundary condition in the derivation of Eq. (19) (i.e., $d > 2r$) may no longer be satisfied (*19*). A more appropriate approach to the problem of solvent reorganizational energy under these conditions may be the ellipsoidal cavity treatment (*20, 21*), where

$$\chi_s = \frac{(\Delta e)^2}{R}\left[\left(\frac{1}{D_{in}} - \frac{1}{D_s}\right)\sum_{n=1}^{\infty}\frac{X_n}{I_n(D_{in}, D_s)} - \left(\frac{1}{D_{in}} - \frac{1}{D_{op}}\right)\sum_{n=1}^{\infty}\frac{X_n}{I_n(D_{in}, D_{op})}\right] \tag{20}$$

and where

$$X_n = 2(2n + 1)\{1 - (-1)^n\}P_n^2(\xi_k)Q_n(\lambda_0)/P_n(\lambda_0) \tag{21}$$

and

$$I_n(D_x, D_y) = 1 - \frac{D_x}{D_y}\left(\frac{\lambda_0 - P_{n+1}(\lambda_0)/P_n(\lambda_0)}{\lambda_0 - Q_{n+1}(\lambda_0)/Q_n(\lambda_0)}\right) \tag{22}$$

$$\lambda_0 - [(A^2/A^2 - B^2)]^{1/2}. \tag{23}$$

In Eqs. (20)–(23), R is the interfocal length, D_{in} is the dielectric constant within the cavity, $\xi_k = d/R$, P_n and Q_n are Legendre polynomials of the first and second kinds, A is the length of the semimajor axis, and B is the length of the two semiminor axes of the ellipsoid.

2. The Comproportionation Equilibrium

The comproportionation constant K_c (*7*) is determined by the equilibrium for class I and II complexes,

$$\text{(II-II)} + \text{(III-III)} \rightleftharpoons 2\text{(III-II)}, \tag{24}$$

and for class III complexes

$$\text{(II-II)} + \text{(III-III)} \rightleftharpoons 2(\text{II}_{1/2}\text{-II}_{1/2}). \tag{25}$$

K_c is usually deduced from the difference in potential between metal-centered reduction couples. For class I and II complexes, K_c is usually less than 10^3 and is determined by contributions from four terms,

$$\Delta G_c = \Delta G_r + \Delta G_e + \Delta G_s + \Delta G_i, \tag{26}$$

where ΔG_c is the free energy of comproportionation, ΔG_r is the free energy of resonance exchange, ΔG_e is the free energy that takes into account the repulsion of like charged metal centers, ΔG_s is an entropic factor ($\frac{1}{2}RT \ln \frac{1}{4}$) that reflects a statistical distribution of Eq. (24), and ΔG_i is an inductive or synergistic factor due to stabilization of M(II) and M(III) or vice versa. For a class I complex, only ΔG_s makes a significant contribution to ΔG_c. For a class II complex, Sutton and Taube (*22*) have shown that all terms can contribute, with ΔG_r being relatively minor and for symmetric systems given by

$$\Delta G_r = H_{ad}^2/E_{op}. \tag{27}$$

It is possible to estimate K_c when it deviates only slightly from the entropic factor of 4 by an amount related to the Coloumb repulsion energy of the metal charges (23). Thus,

$$K_c = 4 \exp(1/\varepsilon r_{mm} kT) \tag{28}$$

where ε is the dielectric constant of the material between the metal atoms separated by the distance r_{mm}.

For class III complexes, K_c is very large. This reflects the strong bonding interaction between donor and acceptor wave functions, which results in delocalization of the odd electron. The greatest contribution to ΔG_c is derived from ΔG_r, where $\Delta H_r = H_{ad}$.

3. *Other Theoretical Approaches*

The Hush model is the preferred method of analysis of mixed valence complexes for the experimentalist because of its readily understandable derivation, its overlap with the Marcus theory of electron transfer, and the facility of its application. However, it is applicable only to weakly coupled class II complexes. A quantitative theory that is applicable to all mixed valence complexes is obviously desirable. Piepho, Krausz, and Schatz (*24*) have developed a vibronic coupling model (PKS model) that is applicable to both class II and III mixed-valence complexes and allows explicit vibronic eigenvalues and eigenvectors to be determined. The PKS model is a two-site, one-dimensional model that uses a valence-bond type of electronic basis and three parameters (ε electron coupling, λ vibronic coupling, and $\bar{\nu}$, the wave number of the totally symmetric metal–ligand stretching vibration, which is usually taken as 500 cm^{-1}). The ε and λ parameters are adjusted so that the position and width of the predicted spectrum match those of the observed spectrum. Buhks (*25*) and Wong and Schatz (*26*) have extended the PKS model to incorporate the motion of solvent as well as the internal motion.

The PKS model has been criticized (*27–29*) for the assumption of a single frequency and its unsatisfactory description of the magnetic circular dichroism (MCD) found for the intervalence band of the Creutz–Taube ion (*30*). In a series of papers (*31*), Ondrechen and coworkers developed a more realistic three-site model for delocalized (class III) bridged mixed-valence complexes. This model incorporates many features of the PKS model but differs in that it explicitly includes the bridge, it uses a molecular orbital basis of one-electron functions, and the choice of important vibrational modes is not the same. The near-IR band line shape of the Creutz–Taube ion has been reasonably

analyzed by using the three-site model, which by interation fits only one Hamiltonian parameter (*31f*). However, the model is appropriate only for delocalized systems.

Piepho has responded to the criticisms of the PKS model by developing an improved version, the MO vibronic coupling model for mixed-valence complexes (*32*). Multicenter vibrations are now considered and a molecular orbital basis set (as with the three-site model) is used. This model was used to calculate band shape and g values for the Cretuz–Taube ion (*33*). The MO vibronic coupling model is admittedly more empirical than the three-site model but it has the advantage in being applicable to all mixed-valence complexes.

In a recent study, Curtis and coworkers (*34*) developed an analysis of electronic coupling in mixed-valence complexes that combines electrochemical results with an extension of Mulliken's theory of donor–acceptor interactions. The approach was applied to class II and near class III complexes. It was found that the degree of electronic coupling in these systems is at least three times that which would be predicted based solely on spectroscopic measurements (Eq. 15 of the Hush model). However, the electronic coupling determined for complexes that were very close to, if not of, class III character was significantly smaller than that predicted by Eq. (16).

B. Class III Mixed-Valence Complexes

1. Class III Criteria

Table I compiles the electrochemical and metal–metal absorption band spectral data of novel mixed-valence complexes (*35–46*) that are good candidates for valence delocalized systems. The decision as to where to draw the line between class II and III mixed-valence complexes is a difficult one to make. The Creutz–Taube ion has undergone an extremely rigorous physical characterization by just about every method known (see below), and it is only recently that the preponderance of evidence strongly favors a class III description. The same degree of examination should be applied to the complexes of Table I to fully justify their class III assignment.

In preparing Table I two criteria were used. First, the comproportionation constant for symmetric mixed-valence complexes should be large. It is important to recognize that for complexes in which the metal–metal distance is small significant contributions to K_c arise from factors other than those associated with metal–metal coupling. Second, the breakdown of Hush theory (*4*) for the spectral properties of MMCT transitions should be apparent. In practice this means that the pre-

TABLE I

RUTHENIUM(III/II) COUPLES, COMPROPORTIONATION CONSTANTS, AND MMCT BAND PROPERTIES OF CLASS III COMPLEXES

Complex	$E_{1/2}$ (V)	ΔE (mV)	K_c	λ_{max} (nm)	$\bar{\nu}_{1/2}$ (cm^{-1})	ϵ_{max} ($M^{-1}\,cm^{-1}$)	Solvent	Ref.
$[\{(NH_3)_4Ru\}_2(\mu\text{-bptz})]^{5+}$	0.69[a] 1.58	890	10^{15}	1450	≈2000	500	Acidic H_2O	*35, 36*
$[\{(bpy)_2Ru\}_2(\mu\text{-bptz})]^{5+}$	1.52[a] 2.02	500	3×10^8	[b]			CH_3CN	*37*
$[\{(bpy)_2Ru\}_2(\mu\text{-abpy})]^{5+}$	1.67[a] 2.22	550	2×10^9	[b]			CH_3CN	*37*
$[\{(bpy)_2Ru\}_2(\mu\text{-adc})]^{3+}$	0.38[a] 0.89	510	4×10^8	1410	2600	7800	$ClCH_2CH_2Cl$	*38*
$[\{(bpy)_2Ru\}_2(\text{di-}\mu\text{-}OCH_3)]^{3+}$	−0.09[c] +0.46	550	3×10^9	1800[d]		≈5000[d]	CH_3CN	*39*
$[\{(bpy)_2Ru\}_2(\text{di-}\mu\text{-}OCH_2CH_3)]^{3+}$	−0.06[c] +0.51	570	6×10^9	[e]			CH_3CN	*39*
$[\{(NH_3)_4Ru\}_2(\mu\text{-dtdp})]^{5+}$	−0.130[a] +0.160	290	8×10^4	1500	1240	4300	H_2O	*40*
$[\{(NH_3)_4Ru\}_2(\mu\text{-dpp})]^{5+}$	0.90[f] 1.29	390	4×10^6	[b]			CH_3CN	*41*
$[(tterpyRu)_2(\mu\text{-tpbp})]^{3+}$	0.50[a] 0.34	160	600	1820	2820	27000	CH_3CN	*42*
$[(tterpyRu)_2(\mu\text{-tppz})]^{5+}$	1.40[a] 1.70	300	10^5	1520			CH_3CN	*43*
$[(NH_3)_5RuNCSRu(NH_3)_5]^{4+}$	0.325[a] 0.575	250	16000	1600	929	331	C_6H_5Cl	*44*
trans-$[\{(NH_3)_4Ru(3,5\text{-}Me_2py)\}_2(\mu\text{-pyz})]^{5+}$	0.220[c] 0.575	355	10^6	1703	1970	3040	CH_3CN	*45, 46*
trans-$[\{(NH_3)_4Ru(3,5\text{-}Me_2py)\}(\mu\text{-pyz})\{(NH_3)_5Ru\}]^{5+}$	0.117 0.536	419	10^7	1624	1980	4300	CH_3CN	*46*
trans-$[\{(NH_3)_4Ru(py)\}_2(\mu\text{-pyz})]^{5+}$	0.242[c] 0.582	340	6×10^5	1685	1850	5940	CH_3CN	*45, 46*
trans-$[\{(NH_3)_4Ru(py)\}(\mu\text{-pyz})\{(NH_3)_5Ru\}]^{5+}$	0.128 0.563	435	10^7	1595	2420	3050	CH_3CN	*46*
trans-$[\{(NH_3)_4Ru(3\text{-}Fpy)\}_2(\mu\text{-pyz})]^{5+}$	0.347[c] 0.669	305	10^5	1690	1940	9100	CH_3CN	*46*
trans-$[\{(NH_3)_4Ru(3\text{-}Clpy)\}_2(\mu\text{-pyz})]^{5+}$	0.351[c] 0.672	321	3×10^5	1692	1940	4360	CH_3CN	*46*
cis-$[\{(NH_3)_4Ru(py)\}_2(\mu\text{-pyz})]^{5+}$	0.260[c] 0.628	368	2×10^6	1648	1770	6000	CH_3CN	*46*
cis-$[\{(NH_3)_4Ru(3\text{-}Fpy)\}_2(\mu\text{-pyz})]^{5+}$	0.336[c] 0.699	363	10^6	1651	1790	4570	CH_3CN	*46*
cis-$[\{(NH_3)_5Ru\}(\mu\text{-pyz})\{Ru(NH_3)_4(3,5\text{-}Me_2py)\}]^{5+}$	0.015[c] 0.440	425	10^7	1597	1760	4160	CH_3CN	*46*

[a] Versus SCE.
[b] Not observed.
[c] Versus ferrocenium/ferrocene couple.
[d] Measured at 240 K.
[e] Not reported.
[f] Versus NHE.

dicted band width of the MMCT band by Hush theory is significantly greater than that seen experimentally, the extinction coefficient ε_{max} is large (usually $>10^3\ M^{-1}\ cm^{-1}$), and $\bar{\nu}_{max}$ is solvent independent.

2. Studies of Class III Mixed-Valence Complexes

a. Metal–Metal Coupling. It might be expected that complexes possessing a large comproportionation constant and metal–metal coupling will have a correspondingly large MMCT extinction coefficient. However, such a correlation should be made with caution. For example, the complex $[\{(NH_3)_4Ru\}_2(\mu\text{-bptz})]^{5+}$ (*35, 36*) has a large K_c (10^{15}) but only a small MMCT ε_{max} (500 $M^{-1}\ cm^{-1}$). In contrast, the complex $[(tterpyRu)_2(\mu\text{-tpbp})]^{3+}$ (*42*) has a relatively small K_c (600) but a large ε_{max} (27,000 $M^{-1}\ cm^{-1}$). In a comparison (*36*) between $[\{(NH_3)_4Ru\}_2(\mu\text{-bptz})]^{5+}$ and the Creutz–Taube ion [MMCT λ_{max} = 1596 nm and ε = 7620 $M^{-1}\ cm^{-1}$ in acetonitrile (*46*)], the authors pointed out that, although the metal–metal distances are the same, the $d\pi$ orbitals in $[\{(NH_3)_4Ru\}_2(\mu\text{-bptz})]^{5+}$ are directed toward the middle of the α-diimine chelate system and are not linearily oriented toward each other as in the Creutz–Taube ion. Exactly how this explains the difference in MMCT extinction coefficient or more quantitatively the oscillator strength was left to speculation. The above examples would seem to be excellent candidates for analysis by the MO vibronic coupling (*33*) and three-site (*31*) models that were discussed previously.

Brant and Stephenson (*47*) have suggested that X-ray photoelectron spectroscopy (PES) can be used to distinquish between strongly and weakly coupled metals in delocalized class III complexes. The PES spectra of Creutz–Taube type complexes show two Ru $3d_{5/2}$ photoionization states of equal intensity and split by 3.4–3.6 eV. This was initially thought to be evidence for class II properties. However Hush (*48*) suggested that this behavior was not inconsistent with class III properties if the delocalized valence orbital is highly polarizable so that under the influence of the localized metal core hole the unpaired electron associated with this orbital becomes trapped and two final states are realized. If the metal–metal coupling in class III complexes grows strong, the polarizability of the delocalized valence orbital is diminished until finally the metal core level spectrum must approach a single final state. This condition was met in the mixed-valence complex $[\{[As(p\text{-tol})_3]_2ClRu\}_2(\mu\text{-Cl})_3]$, for which in the PES spectrum only one Ru $3d_{5/2}$ photoionization state was observed (*47*).

b. Nature of the Bridging Ligand. Whether a class II or class III mixed-valence complex is formed obviously depends a great deal on

the nature of the bridging ligand. To be effective, the molecular orbitals of the bridging ligand must be symmetry and energy matched and interact simultaneously with the donor and acceptor orbitals of the metal ions. Having framed the requirements in this way, it is easy to see why in class III complexes the bridging ligands all involve extended π systems. An examination of class III complexes in Table I and in the Creutz review (*7*) shows that there are two main types of bridging systems. The nitrogen donor atom heterocyclic bridging ligands are π acceptors. This means that the Ru(II) π-donor wave function can extend onto the π LUMO of the bridging ligand and the dominant mechanism for metal–metal coupling is called electron transfer superexchange. Conjugated anion bridging ligands are π donors. This allows the Ru(III) π-acceptor wave function to extend itself onto the π HOMO of the bridging ligand and the dominant mechanism for metal–metal coupling is then called hole-transfer superexchange. The above descriptions are rather simplistic. Theoretical studies (*49–51*) show that metal–metal coupling is mediated by the full set of bonding and antibonding orbitals of the bridging ligand. The superexchange pathways described above are those which are expected to make the greatest contribution to metal–metal coupling.

If Ru orbitals closely match the energy of the HOMO or LUMO of the bridging ligand, covalency is approached and the distinction between formal oxidation states becomes blurred, resulting in the extreme case of a radical bridging ligand. The situation is illustrated below:

$$\underset{\text{I}}{M^{2+}\text{—L—}M^{3+}} \longleftrightarrow \underset{\text{II}}{M^{2+}\text{—}L^{+}\text{—}M^{2+}} \longleftrightarrow \underset{\text{III}}{M^{3+}\text{—L—}M^{2+}}. \qquad (29)$$

For the complex $[\{(bpy)_2Ru\}_2(\mu\text{-adc})]^{3+}$ (*38*), researchers invoked a contribution of resonance form II to the ground state in order to explain ESR and electronic absorption spectroscopy results. Alternatively, if Ru orbitals closely match the energy of the LUMO of the bridging ligand, the following resonance forms may result:

$$\underset{\text{I}}{M^{2+}\text{—L—}M^{3+}} \longleftrightarrow \underset{\text{IV}}{M^{3+}\text{—}L^{-}\text{—}M^{3+}} \longleftrightarrow \underset{\text{III}}{M^{3+}\text{—L—}M^{2+}}. \qquad (30)$$

Elaborations of these basic concepts can be found in studies of the comproportionation constant of mixed-valence complexes (*37, 52, 53*).

It is a synthetic challenge for the inorganic coordination chemist to construct class III systems whose ground states have a significant

contribution from resonance forms II or IV. These systems will have properties that will be directly applicable to the construction of molecular materials and devices.

c. Nature of the Ruthenium Ion. The energy of Ru(II) donor and Ru(III) acceptor orbitals and the ability of these orbitals to interact with the bridging ligand can be significantly affected by the nature of the ligands which make up the coordination sphere. It is well known that the potential of the Ru(III/II) couple becomes increasing anodic with increasing coordination of π acceptor ligands [the $[Ru(NH_3)_6]^{3+/2+}$ couple = 0.051 V (*54*), whereas the $[Ru(bpy)_3]^{3+/2}$ couple = 1.272 V vs NHE in aqueous solution (*55*)]. It follows from the previous discussion that symmetric mixed-valence complexes are more likely to have delocalized valency if the $(NH_3)_5Ru(II)$ moiety is bonded to a π acceptor bridging ligand and if a $(diimine)_nRu(III)$ moiety is bonded to a π donor bridging ligand.

In an impressive body of work, Curtis and coworkers (*45, 46*) have synthesized derivatives of the Creutz–Taube ion to probe the influence of the coordination sphere on the magnitude of metal–metal coupling. Class III properties could be transformed to class II properties, simply by changing an ammine ligand to a strong π-acceptor ligand. Both the increase in MMCT band $\Delta\bar{\nu}_{1/2}$ (as shown in Fig. 4) and the decrease in extinction coefficient were consistent with a transformation to class II properties. In addition, the symmetric complexes $[LRu(NH_3)_4(\mu\text{-pyz})\text{-}Ru(NH_3)_4L]^{5+}$ (*46*) have smaller MMCT $\Delta\bar{\nu}_{1/2}$ compared with their asymmetric analogues. This suggests that asymmetry helps trap out the odd electron and promotes conversion to class II properties. Similar effects are seen due to outer-sphere perturbations (discussed below). Examination of these Creutz–Taube derivatives using Piepho's MO vibronic coupling model (*32*) would be a good test of the model and, if successful, could reveal some important details concerning the dependence of metal–metal coupling on the nature of the metal atom as perturbed by its coordination sphere.

Modification of metal–metal coupling is not just restricted to the inner coordination sphere. Hupp and coworkers (*56*) have shown that addition of the crown ethers, dibenzo-36-crown-12 (DB-36-C-12) or dibenzo-30-crown-10 (DB-30-C-10), to a nitromethane solution of the Creutz–Taube ion or *trans*-$[\{(NH_3)_4Ru(py)\}_2(\mu\text{-pyz})]^{5+}$ can result in dramatic changes to the MMCT band because of the affinity of the crown ether oxygens for ruthenium-ammine hydrogens. Figure 5 shows the changes observed for the MMCT of *trans*-$[\{(NH_3)_4Ru(py)\}_2(\mu\text{-pyz})]^{5+}$. The maximum effects occur with the 1 : 1 stoichiometry of crown ether

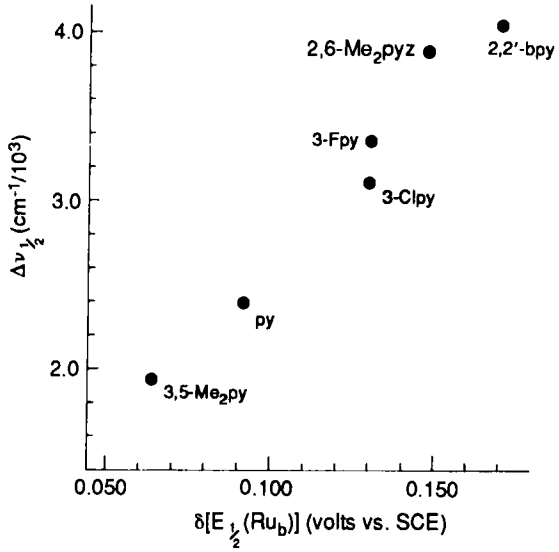

FIG. 4. $\Delta\bar{\nu}_{1/2}$, the band width at half-maximum for the MMCT band vs $\delta[E_{1/2}(Ru_b)]$, the potential shift in the second redox wave relative to the Creutz–Taube second wave for complexes *trans*-$[L(NH_3)_4Ru(\mu\text{-pyz})Ru(NH_3)_5]^{5+}$, where L = 3,5-$Me_2$py, py, 3-Clpy, 3-Fpy, 2,6-Me_2pyz, and bpy. [Reproduced with permission from Ref. (*45*). Copyright (1985) American Chemical Society.]

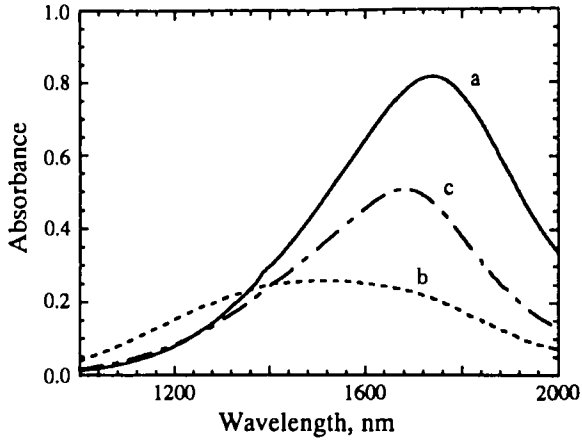

FIG. 5. MMCT absorption spectra for 8.6 m*M* of *trans*-$[\{(NH_3)_5Ru(py)\}_2(\mu\text{-pyz})]^{5+}$ in nitromethane-d_3 with (a) no added crown, (b) 1 eq. of DB-36-C-12, and (c) 16 eq. of DB-36-C-12 (*56*). [Reproduced with permission from Ref. (*45*). Copyright (1985) American Chemical Society.]

to complex. It was suggested that the initially delocalized class III complex becomes valence-localized class II with the formation of the asymmetric 1 : 1 adduct. Further addition of crown ether forms the symmetric 2 : 1 adduct and a return to class III properties. Roberts and Hupp (*57*) have seen a similar affect although not as dramatic by adding dimethyl sulfoxide to an acetonitrile solution of *trans*-$[\{(NH_3)_4Ru(py)\}_2(\mu\text{-pyz})]^{5+}$. The changes in the intervalence spectrum of the complex were suggested to arise from a valence-trapped ground state due to the selective solvation of ammines bonded to Ru(III). Importantly, the Creutz–Taube ion's intervalence transition was largely insensitive to DMSO concentration and this may reflect the magnitude of metal–metal coupling in this complex.

d. Physical Characterization of the Creutz–Taube Ion, $[(NH3)_5Ru\text{-}(\mu\text{-}pyz)Ru(NH_3)_5]^{5+}$. The controversy concerning the classification of the electronic structure of the Creutz–Taube ion appears to have reached a consensus view in favor of the delocalized class III description. A number of studies (*17, 18, 58–66*) have appeared since the Creutz review (*7*) and these have been summarized in Table II. The near-IR, IR, and MCD spectra of the Creutz–Taube ion are of particular interest because of theoretical predictions of low-energy tunneling transitions near 2000 and 3200 cm^{-1} (*30, 67*). FTIR spectroelectrochemistry of the

TABLE II

THE CLASSIFICATION OF THE ELECTRONIC STRUCTURE OF $[\{(NH_3)_5Ru\}_2(\mu\text{-pyz})]^{5+}$

Experiment	Conditions	Time resolution	Year	Conclusion	Ref.
Far IR	6 K Docosane mull	10^{-13}	1981	Delocalized	*58*
Mossbauer, X ray, EPR		10^{-18}–10^{-7}	1984	Delocalization is possible	*59*
EPR	Single crystal 3 K	10^{-9}	1984	Delocalization is possible	*60*
X ray	100 K, 295 K	10^{-18}	1985	Delocalized	*61*
IR and MCD	1.4 K In polymer support	10^{-13}	1986	Delocalized	*62, 63*
Solvent dependence	Room temperature	10^{-13}	1987	Delocalized	*64*
Mossbauer	Liquid He temperature	10^{-7}	1989	Delocalized	*65*
Near and middle IR	D_2O solution	10^{-13}	1989	Delocalized	*66*
Electroabsorption	50% Glycerol/H_2O Liquid N_2	10^{-13}	1989–1991	Delocalized	*17, 18*

complex in D_2O (*66*) showed a broad band at ca. 2000 cm^{-1} (ε = 300 M^{-1} cm^{-1} and $\Delta\bar{\nu}_{1/2}$ = 1400 cm^{-1}) together with a suggestion of a band between 4500 and 5000 cm^{-1}. The latter band is partially obscured by the intense 6320-cm^{-1} absorption but appears to have a band width and an intensity similar to that of the 200-cm^{-1} absorption. A near-IR MCD spectrum of the Creutz–Taube ion in a PVA foil (*63*) showed a weak *C* term in the region of the main band at 6400 cm^{-1}. The MCD intensity was consistent with an approximately 1% or greater (*XY*) polarization of the absorption intensity with *Z*-polarized (metal–metal axis) intensity dominant. The band at 2000 cm^{-1} was also MCD active (*62*), in agreement with electronic coupling models (*30, 31e*).

C. Class II Mixed-Valence Complexes

1. *General Description*

There have been numerous class II mixed-valence complexes synthesized since the Creutz review (*7*). Tables III and IV are compilations of symmetric deca- or octaamminediruthenium (*68–80*) and tetrakisdiiminediruthenium complexes (*37, 41, 81–90*), respectively. Table V is a compilation of asymmetric mixed valence complexes (*45, 46, 77, 83, 86, 87, 91–102*). Table VI summarizes the Hush theory treatments of mixed-valence complexes that have appeared in the literature. A class II valence trapped complex is generally recognized by its small comproportionation constant (K_c is usually <1000), the weak intensity of its MMCT absorption band, a value of $\Delta\bar{\nu}_{1/2}$ that is greater than the values given by either Eq. (2) or (4) (see Table VI), and MMCT energy that is sensitive to the nature of the solvent. The experimental band width for a class II is usually greater than the theoretical bandwidth because of anharmonicity and other effects, such as a significant spin-orbit term for ruthenium systems (1000 cm^{-1}) (*103*). When the experimental $\Delta\bar{\nu}_{1/2}$ is less than or equal to the theoretical $\Delta\bar{\nu}_{1/2}$, class III behavior is approached and electroabsorption spectroscopy (*17, 18, 104*) would seem to be the best method to unimbiguously establish the degree of delocalization.

2. *Studies of Class II Mixed-Valence Complexes*

a. Electroabsorption (Stark Effect) Spectroscopy. The recent application of electroabsorption spectroscopy to the MMCT bands of mixed-valence complexes is an important development (*17, 18, 104*). An external electric field will perturb the electronic/vibronic absorption envelope of an MMCT band in a manner, which is directly relatable to

TABLE III

COMPROPORTIONATION CONSTANTS AND MMCT BAND PROPERTIES OF SYMMETRIC CLASS II COMPLEXES, $[\{(NH_3)_nRu\}_2(\mu\text{-L})]^{m+}$

Complex	K_c	λ_{max} (nm)	ϵ_{max} (M^{-1} cm^{-1})	$\bar{\nu}_{1/2}$ (cm^{-1})	Solvent	Ref.
$[\{(NH_3)_5Ru\}_2(\mu\text{-dpb})]^{5+}$		1040	1430	4900	NO_2Ph	*68*
$[\{(NH_3)_5Ru\}_2(\mu\text{-dph})]^{5+}$		1110	1250	4700	NO_2Ph	*68*
$[\{(NH_3)_5Ru\}_2(\mu\text{-dpo})]^{5+}$		≈1000	≈1220	≈4800	NO_2Ph	*68*
$[\{(NH_3)_5Ru\}_2(\mu\text{-dpph})]^{5+}$		[a]	≈160[b]		CH_3CN	*69*
$[\{(NH_3)_5Ru\}_2(\mu\text{-dpdph})]^{5+}$		[a]	≈16[b]		CH_3CN	*69*
$[\{(NH_3)_5Ru\}_2(\mu\text{-3-dpph})]^{5+}$		[a]	≈0.4[b]		CH_3CN	*69*
$[\{(NH_3)_5Ru\}_2(\mu\text{-azpy})]^{5+}$	40	≈1400	≈500		D_2O	*70*
$[\{(NH_3)_5Ru\}_2(\mu\text{-bphy})]^{5+}$		≈1200	≈40		D_2O	*70*
$[\{(NH_3)_4Ru(isn)\}_2(\mu\text{-dts})]^{5+}$	≈10	≈1008	48		0.2 *M* DCl	*71*
$[\{(NH_3)_5Ru\}_2(\mu\text{-dtsd})]^{5+}$	≈4	808	9 ± 1	6400	0.2 *M* DCl	*72*
$[\{(NH_3)_5Ru\}_2(\mu\text{-dtst})]^{5+}$	≈4	690	2.3 ± 0.7	7000	0.2 *M* DCl	*72*
$[\{(NH_3)_5Ru\}_2(\mu\text{-dcpy})]^{3+}$	1.2×10^5	1510	430		D_2O	*73*
$[\{(NH_3)_5Ru\}_2(\mu\text{-fum})]^{5+}$	55	975	150	5040	CH_3CN	*74*
$[\{(NH_3)_5Ru\}_2(\mu\text{-dcy})]^{4+}$	340	1100	2820	6200	0.1 *M* DCl	*75, 7*
$[\{(NH_3)_4RuPy\}_2(\mu\text{-dcy})]^{4+}$	155	1220	2530	6000	0.1 *M* DCl	*75*
$[\{(NH_3)_4Ru(isn)\}_2(\mu\text{-dcy})]^{4+}$	75	1250	2300	5950	0.1 *M* DCl	*75*
$[\{(NH_3)_5Ru\}_2(\mu\text{-dpmn})]^{5+}$	≈10	990	1600		DMF	*76*
$[\{(NH_3)_5Ru\}_2\{\mu\text{-C(CN)}_3\}]^{4-}$	2400	1550	6200	3700	1 *M* D_2SO_4	*76*
$[\{(NH_3)_5Ru\}_2(\mu\text{-pym})]^{5+}$	343	1400	41	6000	1 *M* D_2SO_4	*77*
$[\{(NH_3)_5Ru\}_2(\mu\text{-12dcb})]^{5+}$	33.2	1058	98	5400	1 *M* D_2SO_4	*77*
$[\{(NH_3)_5Ru\}_2(\mu\text{-13dcb})]^{5+}$	11.2	752	8	5860	1 *M* D_2SO_4	*77*
$[\{(NH_3)_5Ru\}_2(\mu\text{-14dcb})]^{5+}$	23.4	862	507	5600	1 *M* D_2SO_4	*77*
$[\{(NH_3)_5Ru\}_2(\mu\text{-15dcn})]^{5+}$	7.0	781	135	5900	1 *M* D_2SO_4	*77*
$[\{(NH_3)_5Ru\}_2(\mu\text{-16dcn})]^{5+}$	8.5	[c]			1 *M* D_2SO_4	*77*
$[\{(NH_3)_5Ru\}_2(\mu\text{-17dcn})]^{5+}$	10	≈770	20	≈6000	1 *M* D_2SO_4	*77*
$[\{(NH_3)_5Ru\}_2(\mu\text{-26dcn})]^{5+}$	10	≈770	140	≈6000	1 *M* D_2SO_4	*77*
$[\{(NH_3)_5Ru\}_2(\mu\text{-27dcn})]^{5+}$	9	[c]			1 *M* D_2SO_4	*77*
$[\{(NH_3)_5Ru\}_2(\mu\text{-13dca})]^{5+}$	10	752	12	≈6000	1 *M* D_2SO_4	*77*
$[\{(NH_3)_5Ru\}_2(\mu\text{-ppdcp})]^{5+}$	4	800		≈6000	1 *M* D_2SO_4	*77*
$[\{(NH_3)_5Ru\}_2(\mu\text{-dicyd})]^{3+}$	10	[c]			D_2O	*78*
$[\{(NH_3)_5Ru\}_2(\mu\text{-Me}_2\text{dicyd})]^{3+}$	28	[c]			D_2O	*78*
$[\{(NH_3)_5Ru\}_2(\mu\text{-Cl}_2\text{dicyd})]^{3+}$	21	[c]			D_2O	*78*
$[\{(NH_3)_5Ru\}_2(\mu\text{-Cl}_4\text{dicyd})]^{3+}$	13	≈1220	≈575	≈4300	D_2O	*78, 7*
$[\{(NH_3)_5Ru\}_2(\mu\text{-dto})]^{5+}$		640	40		Acetone	*80*
$[\{(NH_3)_5Ru(2,6\text{-Me}_2\text{pz})\}_2(\mu\text{-pz})]^{5+}$	5.4×10^4	1690	1525	3310	CH_3CN	*46*
$[\{(NH_3)_3Ru(bpy)\}_2(\mu\text{-pyz})]^{5+}$	7730	1140	920	4010	CH_3CN	*46*

[a] Broad and ill defined from 850 to 1500 nm.

[b] Not corrected for comproportionation constant.

[c] No MMCT band was observed.

TABLE IV

COMPROPORTIONATION CONSTANTS AND MMCT BAND PROPERTIES OF SYMMETRIC CLASS II COMPLEXES. $[\{(DIIMINE)_2Ru\}_2(\mu\text{-}L)]^{n+}$

Complex[a]	K_c	λ_{max} (nm)	ε_{max} (M^{-1} cm^{-1})	$\bar{\nu}_{1/2}$ (cm^{-1})	Ref.
$[\{(bpy)_2Ru\}_2(\mu\text{-bpt})]^{4+}$	10^5	1800	2400	3300	*81*
$[\{(bpy)_2Ru\}_2(\mu\text{-bpzt})]^{4+}$	10^5	1850	2200	4200	*81*
$[\{(bpy)_2Ru\}_2(\mu\text{-mbpt})]^{4}$	10^5	1850	2400	4170	*81*
$[\{(bpy)_2Ru\}_2(\mu\text{-BiBzIm})]^{3+}$	8.2×10^4	1062	1300		*82–84*
		1950	3400	2300	
$[\{(Me_2bpy)_2Ru\}_2(\mu\text{-BiBzIm})]^{3+}$	9×10^4	1011	1700		*83*
		2000	4650		
$[\{(bpy)_2Ru\}_2(\mu\text{-bpbimH}_2)]^{5+}$		1370	<100	3100	*85*
$[\{(bpy)_2Ru\}_2(\mu\text{-bpbim})]^{3+}$		1700	2000	2520	*85*
$[\{(bpy)_2Ru\}_2(\mu\text{-bpm})]^{5+}$	748	2000			*86*
$[\{(bpy)_2Ru\}_2(\mu\text{-BiIm})]^{3+}$	5.6×10^5	[b]			*84*
$[\{(bpy)_2Ru\}_2(\mu\text{-bppz})]^{5+}$	2000	[b]			*37*
$[\{(bpy)_2Ru\}_2(\mu\text{-dpp})]^{5+}$	1600	[b]			*41*
$[\{(bpy)_2Ru\}_2(\mu\text{-dcpy})]^{3+}$	1100	[b]			*73*
$[\{(bpy)_2Ru\}_2(\mu\text{-dpq})]^{5+}$	510	[b]			*87*
$[\{(phen)_2Ru\}_2(\mu\text{-dpq})]^{5+}$	3400	[b]			*87*
$[\{(bpy)_2Ru\}_2(\mu\text{-dpimbH}_2)]^{5+}$	22	1639	1000	4340	*88*
$[\{(bpy)_2Ru(OH_2)\}_2(\mu\text{-chd})]^{3+}$[c]		910	42	16900	*89*
$[\{(phen)_2RuCl\}_2(\mu\text{-pyz})]^{5+}$	49	1320	650	5000	*90*
$[\{(NO_2phen)_2RuCl\}_2(\mu\text{-pyz})]^{5+}$	49	1270	458	4500	*90*
$[\{(Me_2phen)_2RuCl\}_2(\mu\text{-pyz})]^{5+}$	49	1330	735	4700	*90*
$[\{(Me_4phen)_2RuCl\}_2(\mu\text{-pyz})]^{5+}$	107	1300	589	4700	*90*
$[\{(tterpy)Ru\}_2(\mu\text{-tptp})]^{5+}$		1580	1618	4008	*43*
$[\{(tterpy)Ru\}_2(\mu\text{-tpptp})]^{5+}$		1295	729	6036	*43*
$[\{(tterpy)Ru\}_2(\mu\text{-tpdptp})]^{5+}$		1150	709	4934	*43*

[a] In acetonitrile except where noted.
[b] A MMCT band was not observed.
[c] In D_2O.

changes in the polarizability ($\Delta\alpha$) and the permanent electric dipole moment ($\Delta\mu$) resulting from the MMCT transition. This will allow unequivocal answers to questions regarding the extent of electronic delocalization and may also reveal and permit characterization of MMCT transitions that overlap with more intense MLCT or LMCT bands.

The change in absorption, $\Delta A(\nu)$, which results from the application of an external electric field, F_{ext}, across a sample of nonoriented and

TABLE V

COMPROPORTIONATION CONSTANTS AND MMCT BAND PROPERTIES OF ASYMMETRIC CLASS II COMPLEXES

Complex[a]	K_c	λ_{max} (nm)	ϵ_{max} (M^{-1} cm^{-1})	$\bar{\nu}_{1/2}$ (cm^{-1})	Solvent	Ref.
$[\{(bpy)_2RuCl\}_2(\mu\text{-NCSe})]^{2+}$	<350	945	450	5445	CH_3CN	91
$[\{(bpy)_2RuCl\}_2(\mu\text{-NCS})]^{2+}$	350	940	411	5464	CH_3CN	92
$[\{(bpy)_2Ru(NCS)\}_2(\mu\text{-NCS})]^{2+}$		735	36	4565	CH_3CN	92
$[\{(bpy)_2Ru(NO_2)\}_2(\mu\text{-NCS})]^{2+}$		820	150	4845	CH_3CN	92
$[(bpy)_2Ru(\mu\text{-BiBzIm})Ru(Me_2bpy)_2]^{3+}$	3.4×10^5	994	1700		CH_3CN	83
		1855	3200			
$[(bpy)_2Ru(\mu\text{-BiBzIm})Ru\{(COOEt)_2bpy\}_2]^{3+}$	3.6×10^5	1030	2100		CH_3CN	83
		1445	2160			
$[(bpy)_2RuCl(\mu\text{-pyzc})Ru(bpy)_2]^{3+}$	3.5×10^3	1140	730	3700	CH_3CN	86
$[Ru_2(OH_2)Cl(CH_3CN)(O_2CC_6H_4\text{-p-}OCH_3)_4]^{2+}$		960	575	4820	$CHCl_3$	93
$[Ru_2(OH_2)Cl(CH_3CN)(O_2CC_6H_5)_4]^{2+}$		920			$CHCl_3$	93
$[Ru_2(OH_2)Cl(CH_3CN)(O_2CC_6H_4\text{-p-}CH_3)_4]^{2+}$		935			$CHCl_3$	93
$[Ru_2(OH_2)Cl(CH_3CN)(O_2CC_6H_4\text{-p-}Cl)_4]^{2+}$		900			$CHCl_3$	93
$[(bpy)_2RuCl(\mu\text{-pyz})Ru(NH_3)_5]^{4+}$	1.2×10^7	1035	1300	5470	CH_3CN	45, 9
$[(bpy)_2RuCl(\mu\text{-pyz})Ru(NH_3)_4(4\text{-Mepy})]^{4+}$	1.0×10^5	1180	1240	5430	CH_3CN	94
$[(bpy)_2RuCl(\mu\text{-pyz})Ru(NH_3)_4(3,5\text{-}Me_2py)]^{4+}$	1.0×10^5	1160	713	5650	CH_3CN	94
$[(bpy)_2RuCl(\mu\text{-pyz})Ru(NH_3)_4(py)]^{4+}$	6.1×10^4	1176	1340	5480	CH_3CN	45, 9
$[(bpy)_2RuCl(\mu\text{-pyz})Ru(NH_3)_4(3\text{-Fpy})]^{4+}$	7.1×10^3	1266	918	5120	CH_3CN	94
$[(bpy)_2RuCl(\mu\text{-pyz})Ru(NH_3)_4(4\text{-Acpy})]^{4+}$	7.1×10^3	1190	518	5440	CH_3CN	94
$[(bpy)_2RuCl(\mu\text{-pyz})Ru(NH_3)_4(3\text{-Clpy})]^{4+}$	5.9×10^3	1308	1082	4950	CH_3CN	45, 9
$[(bpy)_2RuCl(\mu\text{-pyz})Ru(NH_3)_4(4\text{-}C(O)NH_2py)]^{4+}$	5.4×10^3	1232	490	5910	CH_3CN	94
$[(bpy)_2RuCl(\mu\text{-pyz})Ru(NH_3)_4(2,6\text{-}Me_2pyz)]^{4+}$	910	1304	868	5360	CH_3CN	94
$[(bpy)_2RuCl(\mu\text{-pyz})Ru(NH_3)_3(bpy)]^{4+}$	510	1313	400	5650	CH_3CN	94
$[(bpy)_2RuCl(\mu\text{-pyz})Ru(NH_3)_3(phen)]^{4+}$	330	1310	826	5940	CH_3CN	94
$[Ru(NH_3)_5(\mu\text{-pyz})Ru(NH_3)_4(3\text{-Clpy})]^{5+}$	5.1×10^7	1490	3400	3180	CH_3CN	45, 9
$[Ru(NH_3)_5(\mu\text{-pyz})Ru(NH_3)_4(3\text{-Fpy})]^{5+}$	4.7×10^7	1508	2420	3350	CH_3CN	45, 9
$[Ru(NH_3)_5(\mu\text{-pyz})Ru(NH_3)_4(2,6\text{-}Me_2pyz)]^{5+}$	4.6×10^7	1346	2430	3880	CH_3CN	45, 9
$[Ru(NH_3)_5(\mu\text{-pyz})Ru(NH_3)_3(bpy)]^{5+}$	4.7×10^7	1153	1650	4040	CH_3CN	45, 9
$cis\text{-}[Ru(NH_3)_5(\mu\text{-pyz})Ru(NH_3)_4(py)]^{5+}$	1.9×10^8	1441	2920	3160	CH_3CN	46
$cis\text{-}[Ru(NH_3)_5(\mu\text{-pyz})Ru(NH_3)_4(3\text{-Fpy})]^{5+}$	3.4×10^8	1541	2790	3370	CH_3CN	46
$[Ru(NH_3)_5(\mu\text{-4cp})Ru(NH_3)_5]^{5+}$	4.4×10^4	1020	1275	4980	CH_3CN	46, 7
$[Ru(NH_3)_5(\mu\text{-3cp})Ru(NH_3)_5]^{5+}$	6370	847	23	5100	1 M D_2SO_4	77
$[Ru(NH_3)_5(\mu\text{-4cp})Ru(NH_3)_4(3,5\text{-}Me_2py)]^{5+}$	1.3×10^6	908	1010	5300	CH_3CN	46
$[Ru(NH_3)_5(\mu\text{-4cp})Ru(NH_3)_4(py)]^{5+}$	3.5×10^6	892	1145	4900	CH_3CN	46
$[Ru(NH_3)_5(\mu\text{-4cp})Ru(NH_3)_4(4\text{-Clpy})]^{5+}$	1.2×10^7	860	560	5170	CH_3CN	46
$[Ru(NH_3)_5(\mu\text{-4cp})Ru(NH_3)_4(4\text{-Brpy})]^{5+}$	1.4×10^7	873	480	5280	CH_3CN	46
$[Ru(NH_3)_5(\mu\text{-4cp})Ru(NH_3)_4(3\text{-Clpy})]^{5+}$	2.2×10^7	860	1000	5320	CH_3CN	46
$[Ru(NH_3)_5(\mu\text{-4cp})Ru(NH_3)_4(3\text{-Fpy})]^{5+}$	1.5×10^7	850	940	5280	CH_3CN	46
$[Ru(NH_3)_5(\mu\text{-4cp})Ru(NH_3)_4(2,6\text{-}Me_2pyz)]^{5+}$	4.9×10^7	840	660	5420	CH_3CN	46
$[\{Ru(NH_3)_4(3,5\text{-}Me_2py)\}_2(\mu\text{-4cp})]^{5+}$	4660	1026	890	5740	CH_3CN	46
$[\{Ru(NH_3)_4(py)\}_2(\mu\text{-4cp})]^{5+}$	6360	1028	1580	4840	CH_3CN	46
$[\{Ru(NH_3)_4(4\text{-Brpy})\}_2(\mu\text{-4cp})]^{5+}$	5240	1050	1780	4850	CH_3CN	46
$[\{Ru(NH_3)_4(4\text{-Clpy})\}_2(\mu\text{-4cp})]^{5+}$	4660	1042	1480	5070	CH_3CN	46
$[\{Ru(NH_3)_4(3\text{-Clpy})\}_2(\mu\text{-4cp})]^{5+}$	4660	1035	1080	5080	CH_3CN	46
$[\{Ru(NH_3)_4(3\text{-Fpy})\}_2(\mu\text{-4cp})]^{5+}$	4480	1033	940	5000	CH_3CN	46
$[\{Ru(NH_3)_4(3\text{-}Me_2pyz)\}_2(\mu\text{-4cp})]^{5+}$	3550	960	450	6050	CH_3CN	46
$[\{Ru(NH_3)_3(bpy)\}_2(\mu\text{-4cp})]^{5+}$	944	994	660	5970	CH_3CN	46
$[\{Ru(NH_3)_5\}_2(\mu\text{-4-C(O)Opy})]^{4+}$	2.7×10^7	720	295	5060	H_2O	95
$[\{Ru(NH_3)_5\}_2(\mu\text{-4-C(O)NHpy})]^{4+}$	1.3×10^9	761	900	4620	H_2O	95
$[Ru(NH_3)_5(\mu\text{-4,4'-bpy})Ru(terpy)(bpy)]^{5+}$		≈640	350	5500	CH_3CN	96
$[(phen)_2Ru(\mu\text{-dpp})Ru(bpy)_2]^{5+}$	2400	[b]			CH_3CN	87
$[(phen)_2Ru(\mu\text{-dpq})Ru(bpy)_2]^{5+}$	1100	[b]			CH_3CN	87
$cis\text{-}[(NH_3)_5RuNCRu(bpy)_2CN]^{3+}$	6×10^{19}	694	3500	4500	H_2O	97
$[(NH_3)_5RuNCRu(CN)_5]^-$	3×10^{16}	675	2840	4520	H_2O	98, 9
$cis\text{-}[py(NH_3)_4RuNCRu(bpy)_2CN]^{3+}$	10^{17}	781	3800	4300	H_2O	97
$[(NH_3)_5Ru(\mu\text{-NC})Ru(\eta^5\text{-cp})(PPh_3)_2]^{3+}$		640	3250	5200	Acetone	100
$[\{(CN)_5Ru\}_2(\mu\text{-CN})]^{6-}$		1094	7000		H_2O	101
$[(NH_3)_5Ru(\mu\text{-pyz})Ru(CN)_5]^0$	1.5×10^8	[b]			H_2O	102

[a] Where geometric isomerism is possible, all complexes are *trans* unless otherwise noted.
[b] Not observed.

TABLE VI

HUSH MODEL CALCULATED PARAMETERS OF CLASS II MIXED-VALENCE COMPLEXES

Complex	$\bar{\nu}_{1/2}$(expt, cm^{-1})	$\bar{\nu}_{1/2}$(calc, cm^{-1})	r (Å)	H_{ab}(cm^{-1})	$\alpha^2 \times 10^3$	Ref.
$[\{(bpy)_2RuCl\}_2(\mu\text{-NCS})]^{2+}$	5464	4959	7	453	1.85	*92*
$[\{(bpy)_2Ru(NCS)\}_2(\mu\text{-NCS})]^{2+}$	4565	5605	7	138[a]	0.10	*92*
$[\{(bpy)_2Ru(NO_2)\}_2(\mu\text{-NCS})]^{2+}$	4845	5307	7	276[a]	0.51	*92*
$[\{(bpy)_2RuCl\}_2(\mu\text{-NCSe})]^{2+}$	5445	4994	7.1	465	1.90	*91*
$[\{(bpy)_2Ru\}_2(\mu\text{-bpt})]^{4+}$	3300	3580	6.184	700	16	*81*
$[\{(bpy)_2Ru\}_2(\mu\text{-bpzt})]^{4+}$	4200	3530	6.184	740	19	*81*
$[\{(bpy)_2Ru\}_2(\mu\text{-mbpt})]^{4+}$	4170	3530	6.184	770	20	*81*
$[\{(bpy)_2Ru\}_2(\mu\text{-BiBzIm})]^{3+}$	2300	3440	5.5	725	20	*82*
$[\{(bpy)_2Ru\}_2(\mu\text{-bpbimH}_2)]^{5+}$	3100	4100[a]	12–15	60–80	0.07–0.12[a]	*85*
$[\{(bpy)_2Ru\}_2(\mu\text{-bpbim})]^{3+}$	2520	3685[a]	12–15	240–300	1.67–2.60[a]	*85*
$[(bpy)_2RuCl(\mu\text{-pyzc})Ru(bpy)_2)]^{3+}$	3700	4300	6.9	456[a]	2.7	*86*
$[\{(bpy)_2Ru\}_2(\mu\text{-dpimbH}_2)]^{5+}$	4340	3780	8	4700[a]	5.9[a]	*88*
$[\{(bpy)_2Ru(OH_2)\}_2(\mu\text{-chd})]^{3+}$	16900	5040	4.60	400	1.3	*89*
$[Ru(NH_3)_5(\mu\text{-dpb})]^{5+}$	4900	4710	15.8	340	1.2[a]	*68*
$[\{Ru(NH_3)_5\}_2(\mu\text{-dpb})]^{5+}$	4700	4560	18.1	260	0.8[a]	*68*
$[\{Ru(NH_3)_5\}_2(\mu\text{-dpo})]^{5+}$	≈4800	≈4810	20.6	≈240	≈0.6	*68*
$[\{Ru(NH_3)_5\}_2(\mu\text{-azpy})]^{5+}$				476–780		*70*
$[\{Ru(NH_3)_5\}_2(\mu\text{-bphy})]^{5+}$				≈266		*70*
$[\{Ru(NH_3)_5\}_2(\mu\text{-dtsd})]^{5+}$	6400	5300	14.4			*72*
$[\{Ru(NH_3)_5\}_2(\mu\text{-dtst})]^{5+}$	7000	5800	17.6			*72*
$[\{phen)_2RuCl\}_2(\mu\text{-pyz})]^{5+}$	5000	4190	6.9	467[a]	3.8[a]	*90*
$[\{NO_2phen)_2RuCl\}_2(\mu\text{-pyz})]^{5+}$	4500	4270	6.9	379[a]	2.3[a]	*90*
$[\{Me_2phen)_2RuCl\}_2(\mu\text{-pyz})]^{5+}$	4700	4160	6.9	478[a]	4.1[a]	*90*
$[\{Me_4phen)_2RuCl\}_2(\mu\text{-pyz})]^{5+}$	4700	4220	6.9	434[a]	3.2[a]	*90*
$[(bpy)_2Ru(\mu\text{-dcpy})Ru(NH_3)_4]^{3+}$	3500	3400	7	279	0.72	*73*
$[\{Ru(NH_3)_5\}_2(\mu\text{-fum})]^{5+}$	5040	4867	10.1	179[a]	0.3[a]	*75*
$[\{Ru(NH_3)_5\}_2(\mu\text{-dcy})]^{4+}$	6200	4580				*75, 76*
$[\{trans\text{-}Ru(NH_3)_4(py)\}_2(\mu\text{-dcy})]^{4+}$	6000	4350				*75*
$[\{trans\text{-}Ru(NH_3)_4(isn)\}_2(\mu\text{-dcy})]^{4+}$	5950	4300				*75*
$[(bpy)_2RuCl(\mu\text{-pyz})Ru(NH_3)_5]^{5+}$	5470		6.9	779[a]	6.5[a]	*94*
$[(bpy)_2RuCl(\mu\text{-pyz})Ru(NH_3)_4(4\text{-Mepy})]^{5+}$	5430		6.9	710[a]	7.0[a]	*94*
$[(bpy)_2RuCl(\mu\text{-pyz})Ru(NH_3)_4(3,5\text{-Me}_2py)]^{5+}$	5650		6.9	550[a]	4.1	*94*
$[(bpy)_2RuCl(\mu\text{-pyz})Ru(NH_3)_4(py)]^{5+}$	5480		6.9	745[a]	7.6	*94*
$[(bpy)_2RuCl(\mu\text{-pyz})Ru(NH_3)_4(3\text{-Fpy})]^{5+}$	5120		6.9	570[a]	5.2	*94*
$[(bpy)_2RuCl(\mu\text{-pyz})Ru(NH_3)_4(4\text{-Acpy})]^{5+}$	5440		6.9	460[a]	3.0[a]	*94*
$[(bpy)_2RuCl(\mu\text{-pyz})Ru(NH_3)_4(3\text{-Clpy})]^{5+}$	4950		6.9	600[a]	6.2	*94*
$[(bpy)_2RuCl(\mu\text{-pyz})Ru(NH_3)_4(4\text{-C(O)NH}_2py)]^{5+}$	5910		6.9	420[a]	2.7	*94*
$[(bpy)_2RuCl(\mu\text{-pyz})Ru(NH_3)_4(2,6\text{-Me}_2pyz)]^{5+}$	5360		6.9	560[a]	5.3[a]	*94*
$[(bpy)_2RuCl(\mu\text{-pyz})Ru(NH_3)_3(bpy)]^{5+}$	5650		6.9	390[a]	2.6[a]	*94*
$[(bpy)_2RuCl(\mu\text{-pyz})Ru(NH_3)_3(phen)]^{5+}$	5940		6.9	575[a]	5.7[a]	*94*
$[\{(NH_3)_5Ru\}_2(\mu\text{-C(CN)}_3\}]^{4+}$	3700	3900				*76*
$[\{(NH_3)_5Ru\}_2\{\mu\text{-4-C(O)Opy}\}]^{4+}$	5060		9	300		*95*
$[\{(NH_3)_5Ru\}_2\{\mu\text{-4-C(O)NHpy}\}]^{4+}$	4620		9	510		*95*
$[\{(NH_3)_5Ru\}_2(\mu\text{-4-cp})]^{5+}$	5170		9.3	525		*77*
$[\{(NH_3)_5Ru\}_2(\mu\text{-3-cp})]^{5+}$	5100		8.2	93		*77*
$[\{(NH_3)_5Ru\}_2(\mu\text{-pym})]^{5+}$	6000	4060	6.0	143		*77*
$[\{(NH_3)_5Ru\}_2(\mu\text{-12dcb})]^{5+}$	5400	4670	5.9	236		*77*
$[\{(NH_3)_5Ru\}_2(\mu\text{-13dcb})]^{5+}$	5860	5540	10.2	50		*77*
$[\{(NH_3)_5Ru\}_2(\mu\text{-14dcn})]^{5+}$	5600	5180	11.8	314		*77*
$[\{(NH_3)_5Ru\}_2(\mu\text{-15dcn})]^{5+}$	5900	5440	12.1	169		*77*
$[\{(NH_3)_5Ru\}_2(\mu\text{-17dcn})]^{5+}$	≈6000	5480	8.1	104		*77*
$[\{(NH_3)_5Ru\}_2(\mu\text{-26dcn})]^{5+}$	≈6000	5480	14.0	148		*77*
$[\{(NH_3)_5Ru\}_2(\mu\text{-ppdcp})]^{5+}$	≈6000	5370	12.0	48		*77*
$[\{(NH_3)_5Ru\}_2(\mu\text{-13dcn})]^{5+}$	≈6000	5540	10.2	62		*77*
$[\{(NH_3)_5Ru\}_2(\mu\text{-Cl}_4\text{dicyd})]^{3+}$	4300	4350	13	<200		*78, 79*
$[\{(bpy)_2Ru\}_2(\mu\text{-tptp})]^{5+}$	4008	3820	11	380		*43*
$[\{(bpy)_2Ru\}_2(\mu\text{-tpptp})]^{5+}$	6036	4220	15.5	240		*43*
$[\{(bpy)_2Ru\}_2(\mu\text{-tpdptp})]^{5+}$	4934	4480	20	180		*43*

[a] Calculated from data provided.

immobilized molecules, can be described (*18*) by a linear combination of zeroth, first, and second derivatives of the absorption band:

$$\Delta A(\nu) = \left\{ A_x \cdot A(\nu) + B_x \cdot \frac{\nu}{1.5\,h} \cdot \frac{d[A(\nu)/\nu]}{d\nu} + C_x \cdot \frac{\nu}{30\,h^2} \cdot \frac{d^2[A(\nu)/\nu]}{d\nu^2} \right\} \cdot F_{\text{int}}{}^2, \tag{31}$$

where $A_x = D/3 + (3\cos^2\chi - 1)E/30$; $B_x = 5F + (3\cos^2\chi - 1)G$; $C_x = 5H + (3\cos^2\chi - 1)I$; $D = S^1$; $E = [3S^2 - 2S^1]$; $F = (\frac{1}{2})\text{Tr}(\Delta\alpha) + \mathbf{R}^1 \cdot \Delta\mu$; $F + G = (\frac{3}{2})\mathbf{m} \cdot \Delta\alpha \cdot \mathbf{m} + \mathbf{R}^2 \cdot \Delta\mu$; $H = |\Delta\mu|^2$; $H + I = 3(\mathbf{m} \cdot \Delta\mu)^2$. χ specifies the experimental angle between the external electric field and the light polarization at frequency ν, and h is Planck's constant. The scalars S^1 and S^2, and the vectors $\mathbf{R}^1$ and $\mathbf{R}^2$ are functions of the transition moment polarizability and hyperpolarizability tensors. $\mathbf{m}$ is a unit vector oriented along the transition dipole moment and F_{int} is the internal electric field at the molecule, which depends on the externally applied field F_{ext} such that

$$F_{\text{int}} = fF_{\text{ext}}, \tag{32}$$

where f is a tensor that corrects for the local electric field and depends on the dielectric constant of the medium.

Figures 6 and 7 show absorption and electroabsorption spectra of $[\{(NH_3)_5Ru\}_2(\mu\text{-pyz})]^{5+}$ and $[\{(NH_3)_5Ru\}_2(\mu\text{-4,4'-bpy})]^{5+}$, respectively. The change in ΔA as a function of χ is uniform for the bands, which indicates that the molecular properties that give rise to ΔA are identically oriented with respect to the transition dipole moment. The electroabsorption spectra in the near-IR region (MMCT bands) give the greatest differences between complexes when analyzed with Eq. (31) and these are shown in Fig. 8. For the Creutz–Taube ion (Fig. 8A), the spectrum does not satisfactorily reduce to a sum of derivatives but nevertheless shows that $\Delta A(\nu)$ line shape to be modeled primarily by a negative zeroth derivative (A_x) term, especially at energies below 6500 cm^{-1}. The fit in this case yields a value for $|\Delta\mu| = 0.7 \pm 0.1$ D, which when compared with the maximum permanent electric dipole moment ($|\Delta\mu|_{\text{max}} = 32.7$ D, assuming a metal-to-metal distance) is strong evidence for a delocalized ground state. Contrast this result with the analysis of the electroabsorption spectrum of $[\{(NH_3)_5Ru\}_2(\mu\text{-4,4'-bpy})]^{5+}$ shown in Fig. 8B.

In Fig. 8B, the linear combination of derivatives closely models the $\Delta A(\nu)$ line shape of the near-IR band. The second-derivative component

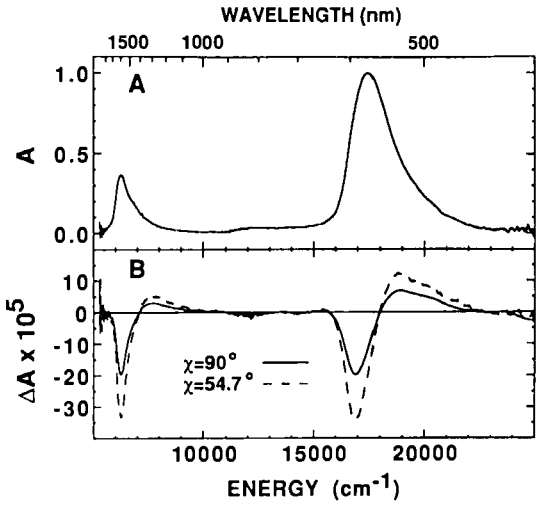

FIG. 6. (A) Absorption and (B) electroabsorption spectra of $[\{(NH_3)_5Ru\}_2(\mu\text{-pyz})]^{5+}$ at $\chi = 90°$ (—) and $\chi = 54.7°$ (---) are shown. Fifty percent glycerol/H_2O, 77 K, $F_{ext} = 4 \times 10^5$ V/cm. [Reproduced with permission from Ref. (*18*). Copyright (1991) American Chemical Society.]

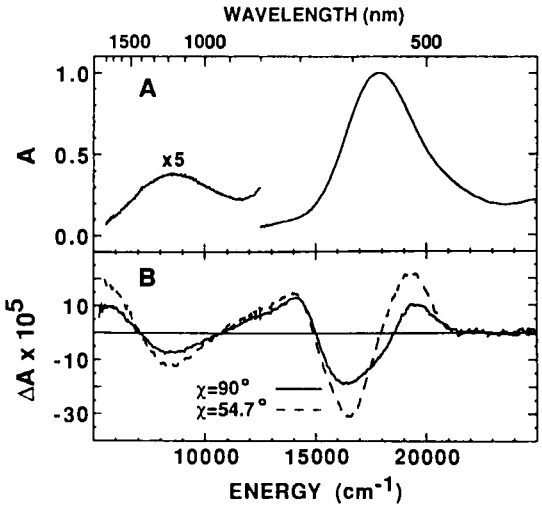

FIG. 7. (A) Absorption and (B) electroabsorption spectra of $[\{(NH_3)_5Ru\}_2(\mu\text{-4,4'-bpy})]^{5+}$ at $\chi = 90°$ (—) and $\chi = 54.7°$ (---) are shown. Fifty percent glycerol/H_2O, 77 K, $F_{ext} = 4 \times 10^5$ V/cm. The near-IR absorption has been magnified 5×. (Reproduced with permission from Ref. (*18*). Copyright [1991] American Chemical Society.)

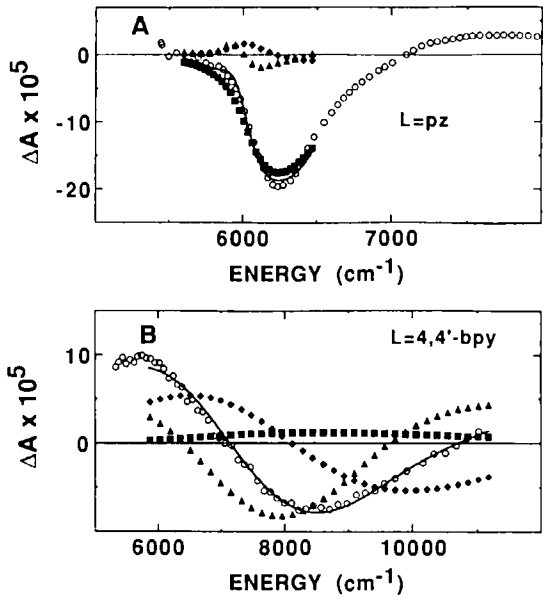

FIG. 8. (A) Fit (—) to electroabsorption data (○) for $[\{(NH_3)_5Ru\}_2(\mu\text{-pyz})]^{5+}$ at $\chi = 90°$ in the near-IR region of the spectrum. Zeroth (■), first (◆), and second (▲) components of the fits are also shown. (B) Fit (—) to electroabsorption data (○) for $[\{(NH_3)_5Ru\}_2(\mu\text{-4,4'-bpy})]^{5+}$ at $\chi = 90°$ in the near-IR region of the spectrum. Zeroth (■), first (◆), and second (▲) components of the fits are also shown. [Reproduced with permission from Ref. (*18*). Copyright (1991) American Chemical Society.]

dominates the spectrum and the fit yields a value for $|\Delta\mu| = 28.5 \pm 1.5$ D, indicating that the states involved are highly dipolar and the unpaired electron is essentially localized. The value of $|\Delta\mu|$ is substantially smaller than $|\Delta\mu|_{max} = 54.3$ D. There are a number of possible explanations of this difference (*11*), but it seems likely that the effective separation R_e between metal ions is reduced by delocalization of the donor wave function onto the bridging ligand.

The consequences of a smaller separation between metal ions has already been discussed in Section II.A.1, where the application of an ellipsoid model for outersphere reorganization energy was introduced. Hush theory calculations of H_{ad} and the mixing coefficient α [in the Creutz review (*7*) and Table VI of this chapter], which use R = metal–metal distance, are largely underestimated. For example, Sutton, Sutton, and Taube (*105*) have reported H_{ad} and α values for $[\{(NH_3)_5Ru\}_2(\mu\text{-4,4'-bpy})]^{5+}$ of 460 cm^{-1} and 0.057 [R = 11.3 Å in Eq. (15)]. Hupp, Dong, Blackbourn, and Lu (*106*) have estimated for the

above complex $R_e = 5.1 \pm 0.7$ Å, which yields $H_{ad} = 1020 \pm 130$ cm^{-1} and $\alpha = 0.126$. Clearly, electroabsorption studies of all class II complexes should be done to get more reasonable estimates of H_{ad} and α.

b. Raman and Electronic Absorption Spectroscopy. The intervalence-enhanced Raman scattering from $[(CN)_5Ru(\mu\text{-}CN)Ru(NH_3)_5]^-$ allowed a mode-by-mode assessment of the Franck–Condon barrier to intramolecular electron transfer (*107*). The results agreed well with X-ray crystallographic measurements. An attempt to apply this technique to the symmetric mixed-valence complexes $[\{(bpy)_2RuCl\}_2(4,4'\text{-}bpy)]^{3+}$ and $[\{(NH_3)_5Ru\}_2(4,4'\text{-}bpy)]^{5+}$ was unsuccessful due to the overlap of MLCT and MMCT bands (*108*). The symmetric $(CN)_5Ru$ analogue proved to be thermally unstable.

The resonance Raman spectrum of *trans*-$[\{(bpy)_2Ru(CN)\}_2(\mu\text{-}CN)]^{2+}$ under near-resonance conditions with the MMCT band showed enhancement of the bridging cyanide stretching as expected for this type of electronic transition (*109*). Analysis of the IR spectrum supports the valence-localized model in contrast to a previous study (*110*).

The broadness of the intervalence electronic absorption band and the lack of structure has generally lent themselves to a rather simplistic singly degenerate state-to-state description. Multiple MMCT transitions have been observed for osmium dimers (*111*), for which the spin orbit coupling term (λ) is large (for Os, $\lambda \simeq 3000$ cm^{-1} and, for Ru, $\lambda \simeq 1000$ cm^{-1}). In addition, the lowering the symmetry of the ruthenium coordination sphere will split the degeneracy of $d\pi$ orbitals and result in multiple MMCT transitions (*112*). These factors may explain the multiple MMCT transitions seen for ruthenium diimine complexes, which incorporate the 2,2-bibenzimidazolate (BiBzIm) bridging ligand (*82, 83*).

c. Solvent Effects. Studies into the solvent dependence of MMCT bands have proven to be especially fruitful in the years since the Creutz review (*7*). According to Marcus–Hush theory, the dependence of E_{op} on the outersphere reorganization energy is given by Eq. (19). Thus, for a given class II mixed-valence complex in which χ_i and $\Delta E'$ in Eq. (17) can be considered solvent independent, shifts in E_{op} with the nature of the solvent should show a linear correlation with $1/D_{op}\text{-}1/D_s$. Figure 9 shows the linear correlation between E_{op} and $1/D_{op}\text{-}1/D_s$ for the complex $[\{(NH_3)_5Ru\}_2(\mu\text{-}4,4'\text{-}bpy)]^{5+}$ (*112*). Similar correlations for other mixed-valence complexes can be found in the literature (*74, 91, 92, 113*). The data point for D_2O is more than three standard deviations above the best-fit line for the remaining solvents. This nonconformity had been ascribed to hydrophobic solvent effects or to solvent-induced nonlocal

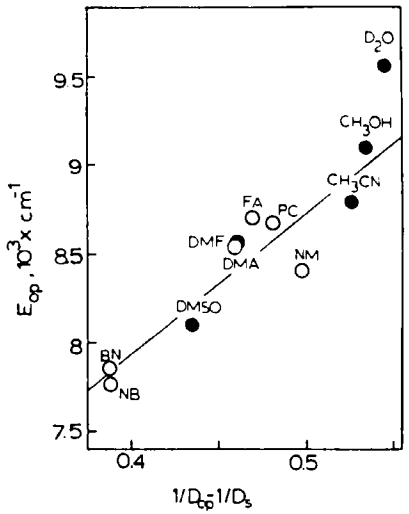

FIG. 9. MMCT band energies vs $1/D_{op} - 1/D_s$. Key to the solvents: BN, benzonitrile; NB, nitrobenzene; DMSO, dimethyl sulfoxide; DMF, dimethylformamide; DMA, dimethylacetamide; PC, propylene carbonate; FA, formamide; NM, nitromethane. [Reproduced with permission from Ref. (*112*). Copyright (1987) American Chemical Society.]

dielectric properties (*114, 115*). However, a plot of MMCT band E_{op} for the complex $[\{(NH_3)_5Ru\}_2(\mu\text{-}4,4'\text{-bpy})]^{5+}$ (at infinite dilution) vs $1/D_{op}$-$1/D_s$ yielded an E_{op} data point for D_2O within two standard deviations of the best-fit line (*106*).

Other solvent studies have shown a dependence of the MMCT band energy on complex concentration, added electrolyte (*116–118*), pressure (*119, 120*), and even the nature of the oxidant used to generate the mixed-valence complex (*121*).

In asymmetric complexes of the type $[(bpy)_2RuCl(\mu\text{-pyz})Ru(NH_3)_4L]^{4+}$, studies (*94*) revealed that there is a solvent donor-number (DN)-dependent contribution to the Frank–Condon barrier of approximately 0.006 eV/DN, which completely overwhelms the dielectric-continuum-theory-derived $(1/D_{op}\text{-}1/D_s)$ solvent dependence typically observed in symmetrical dimers. In this case, variations in MMCT E_{op} with solvent give linear correlations when plotted against solvent dependent $\Delta E_{1/2}$, the difference in potential between the two ruthenium(III/II) couples, as shown in Fig. 10. The microscopic origin of this solvent effect was described by Curtis, Sullivan, and Meyer (*122*) in their study of solvatochromism in the charge transfer transitions of mononuclear Ru(II) and Ru(III) ammine complexes. The dependence

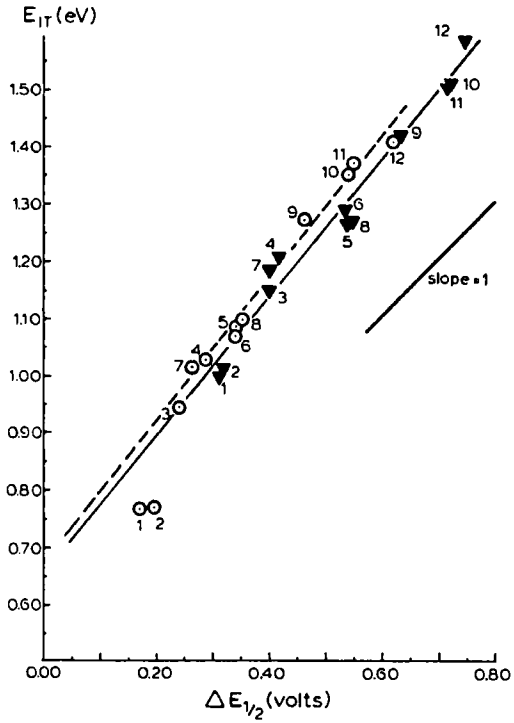

FIG. 10. E_{it} (or E_{op}) vs $\Delta E_{1/2}$ as solvent is varied for the complexes $[(bpy)_2RuCl(\mu\text{-pyz})Ru(NH_3)_4L]^{4+}$, where L = NH_3 (▼) and L = pyridine (⊙). [Reproduced with permission from Ref. (*94*). Copyright (1986) American Chemical Society.]

of charge transfer E_{op} on DN suggested a hydrogen-bonding type of interaction involving the solvent's nonbonding electrons and the N—H bond. The strength of this hydrogen-bonding interaction will depend on the acidity of ammine hydrogen, which is greater for an ammine bound to a Ru(III) ion. The net effect of this interaction is the transfer of electron density from the partially deprotonated ammine to the ruthenium ion. Thus, for the asymmetric mixed-valence complexes in Fig. 10, the Ru(III) oxidation state is stabilized by strong donor solvents and $\Delta E_{1/2}$ increases with increasing DN. An additional consequence is that the solvent stabilization of the Ru(III) coordination sphere must decrease delocalization of the odd electron and the magnitude of metal–metal coupling. Preferential solvation of the Ru(III) coordination sphere in the asymmetric mixed-valence complex $[(bpy)_2RuCl(\mu\text{-pyz})Ru(NH_3)_4L]^{4+}$ by DMSO in acetonitrile was found to make a solvent trapping barrier, which must be considered in situations involv-

ing electron transfer processes of preferentially solvated solutes (*123, 124*). The proper choice of ligands in the design of the complex *trans*-$[(py)(NH_3)_4Ru(\mu\text{-}4cp)Ru(bpy)_2Cl]^{4+}$ permitted the study of solvent-induced or crown-ether-induced redox isomerization (*125*). Preferential solvation also occurs for symmetric ruthenium ammine mixed-valence complexes (*118, 126*), because the solvent's interaction with the Ru(III) ammine coordination sphere is greater than that for Ru(II). Crown ethers were shown to have the same effect (*127*). Hupp (*128*) examined the effect of solvent on the extent of electronic coupling involving complexes of the type $[(bpy)_2RuCl(\mu\text{-}pyz)Ru(NH_3)_4L]^{4+}$. Electronic coupling increased with decreasing solvent-perturbed E_0 [Eq. (3)]. In an unexpected result for a π acceptor bridging ligand, these solvent effects were rationalized (in part) by a hole-transfer pathway for metal–metal coupling.

The thermochromism of MMCT bands has been the subject of recent investigation (*129–131*). The MMCT band of asymmetric class II complexes was shown to shift to higher energy with decreasing temperature, whereas for symmetric class II complexes only a negligible temperature dependence was observed. This effect was shown to arise mainly from the temperature dependence of the redox asymmetry term E_0 in Eq. (3). Importantly, the MMCT bands of symmetric and asymmetric class III complexes show only a slight temperature dependence (*113*). It was speculated that this was due to a weak temperature dependence of H_{ad}.

d. Distance between Ruthenium Ions. From electron transfer theory (*10, 132*), the distance dependence of the electron exchange integral H_{ad} obeys the relationship

$$H_{ad} \propto \exp -\beta d, \tag{34}$$

where β is a measure of the electron transmitting properties of the bridging medium and d is the separation between donor and acceptor wave functions. Thus, for a series of bridging ligands in which the value of β is constant, an exponential dependence of H_{ad} on the distance of separation is expected. Figure 11 shows the distance dependence of H_{ad} for a series of mixed-valence complexes (*77*) of the type $[\{(NH_3)_5Ru\}_2(\mu\text{-}L)]^{5+}$. A similar relationship was found for a series of mixed-valence complexes of the general type $[(NH_3)_5Ru\text{-}py\text{-}(CH{=}CH)_n\text{-}py\text{-}Ru(NH_3)_5]^{5+}$, where py is pyridine (*68, 133*). Reimers and Hush reanalyzed the raw experimental data for these complexes (*23*) and deconvoluted the electronic spectra into contributions from $\pi \rightarrow \pi^*$, metal-

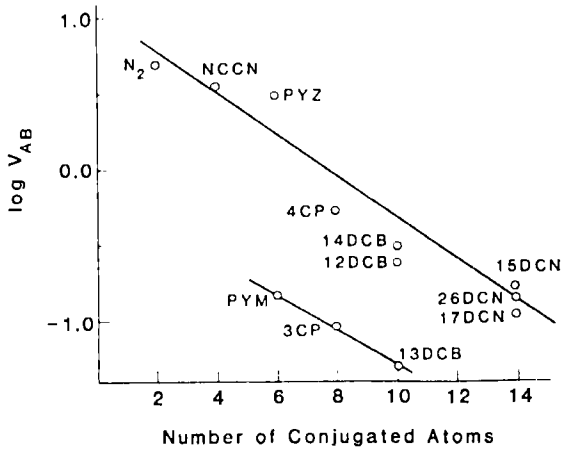

FIG. 11. Plot of log V_{AB} (or H_{ad}) vs number of conjugated atoms in the bridging ligand for complexes of the type $[\{(NH_3)_5Ru\}_2(\mu\text{-L})]^{5+}$. [Reproduced with permission from Ref. (77). Copyright (1983) American Chemical Society.]

to-ligand, ligand-to-metal, and intervalence transitions. Metal–metal separation was increased from 8 to 20 Å in mixed-valence complexes of the type $[\{(NH_3)_5Ru\text{-py-}(Ph)_n\text{-py-}Ru(NH_3)_5]^{5+}$, where Ph is phenyl (*69*). Only weak coupling was observed and it was concluded that aromatic spacers alone are not sufficient to promote strong electronic coupling. Beratan and Hopfield (*134*) developed a semiempirical theory to predict the dependence of H_{ad} on distance and linker geometry for mixed-valence dithiaspirocyclobutane molecules (*72*). Siddarth and Marcus (*135*) applied an extended Huckel method to evaluate H_{ad} for the mixed-valence dithiaspirocyclobutane molecules and obtained somewhat better agreement with experiment.

For a series of similar class II mixed-valence complexes that differ only in the nature of the bridging ligand, MMCT band energy will increase with increasing distance between the metal ions. This dependence has its origin in the magnitude of χ_0 as described by Eq. (19) and has been the subject of study (*136, 137*). The relationship between E_{op} and the barrier to thermal electron transfer [Eq. (1)] was nicely demonstrated by a correlation between electron-transfer rate constants and intervalence-transfer energies (*138*) and is shown in Fig. 12.

e. Nature of the Bridging Ligand. As shown in Fig. 11, Richardson and Taube (*77*) demonstrated the dependence of H_{ad} on the distance of metal–metal separation. The observed trends were predicted theoretically by combining a molecular orbital description of the bridging li-

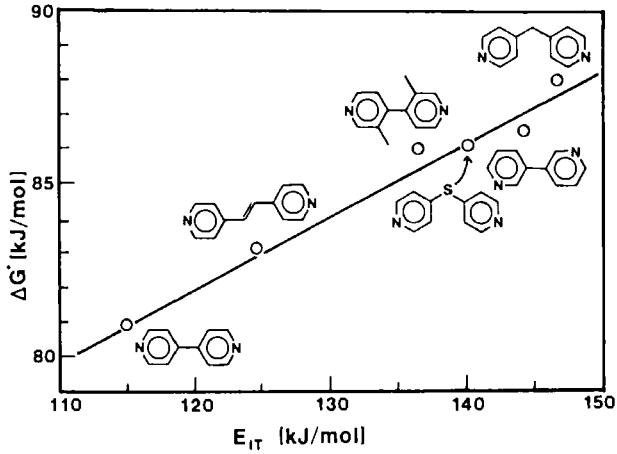

FIG. 12. Plot of activation free energy for electron transfer in $[(H_2O)(NH_3)_4Ru^{II}—L—Co(NH_3)_5]^{5+}$ vs intervalence band energy in $[(NH_3)Ru^{II}—L—Ru^{III}(NH_3)_5]^{5+}$ for six bridging ligands. [Reproduced with permission from Ref. (*138*). Copyright (1987) American Chemical Society.]

gand with a semiempirical measure of metal–ligand charge-transfer interactions. In addition to the distance between metal ions, the dependence of metal–metal coupling on bridging ligand size, orientation of substituents, and saturation was also demonstrated theoretically and experimentally. Hale and Ratner (*139*) reexamined these systems and split up the MMCT transition moments into contributions from hole-transfer and electron-transfer superexchange mechanisms.

Simple modifications of the bridging ligand can have dramatic results. For example, the bridging ligand 4,4′-azopyridine (azpy) is a far poorer medium for metal–metal coupling (*70*) compared with 4,4′-dithiodipyridine (dtdp) (*40*), and this difference is deserving of a theoretical analysis. Joachim (*140*) has explored theoretically the effect of donor and acceptor substitution of the bridging ligand 1,4-dicyanobenzene on through-bond electronic coupling. Recently, there has been surge of interest in anionic π aromatic bridging ligands (*76, 78, 79, 81–85, 88, 91, 92, 95, 141*). The dominant pathway in these systems is expected to be hold-transfer superexchange. In saturated systems (*121, 134*) without the possibility of direct metal–metal orbital overlap, the superexchange pathway is most likely via the σ-symmetry HOMO. These systems provide an advantage in that metal–metal coupling can

be investigated for both Ru(II)–Ru(III) and Ru(III)–Ru(III) complexes. This will be discussed in Section III.B.

f. Transient Absorption Studies. For the mixed-valence complexes $[(dpte)_2ClRu(\mu\text{-}L)RuCl(bpy)_2]^{3+}$ [dpte, $PhSCH_2CH_2SPh$; L, 4,4′-bpy, *trans*-12-bis(4-pyridyl)ethylene, and 1,2-bis(4-pyridyl)ethane], photolysis into the $\pi^* \leftarrow d\pi[Ru^{II}Cl(dpte)_2]$ chromophore resulted in population of the bpy-based ^{3}MLCT excited state $[\text{-}Ru^{III}Cl(bpy^-)bpy]^*$ (*142, 143*). Thus, ligand-to-ligand electron transfer, $[(dpte)_2ClRu^{III}(\mu\text{-}L^-)\text{-}Ru^{III}Cl(bpy)_2]^{3+*} \rightarrow [(dpte)_2ClRu^{III}(\mu\text{-}L)Ru^{III}Cl(bpy^-)bpy)]^{3+*}$, occurred and is competitive with excited-state nonradiative decay by ligand to metal electron transfer.

Picosecond infrared studies (*144–146*) of the dynamics of $[(NC)_5\text{-}Ru^{II}CNRu^{III}(NH_3)_5]^{1-}$ following MMCT photolysis permitted observation of the formation and decay of the MMCT excited state and the evaluation of vibronic coupling and energy-transfer dynamics. The experimental results were in agreement with recent electron-transfer theories that have been used to predict excited vibrational populations resulting from back electron transfer in the Marcus "inverted region" (*146*).

g. Molecular Electronics and Molecular Materials. The purposeful construction of a single supermolecule for signal processing is a practical application of mixed-valence complexes and a major synthetic challenge. The control of signal transfer (an electron) from one metal site to another obviously depends on control of metal–metal coupling. Theoretical studies have focussed on the effect of photoinduced conformational changes of the bridging ligand on the interaction between metals (*147*). The effect on metal–metal coupling must be extreme to be useful because a change in conformation can open new coupling pathways, which although not as efficient serve to diminish the effect (*148*). Chemical approaches such as protonation of the bridging ligand (*70, 85, 149*) or outer-sphere coordination of crown ethers (*57*) are too slow to be of much use. A photoinduced conformational change that causes an outer-sphere perturbation might be a possible approach. Sano and Taube (*80*) prepared [1,5-dithiacyclooctane 1-oxide)bis(pentaammineruthenium)]$^{5+}$, which upon oxidation underwent linkage isomerism. The process was reversible and is an example of molecular hysteresis with potential application to high-density memory storage.

Novel molecular materials may be prepared by considering a mixed-valence complex as a molecular building block. Polymerization and

retention of electron delocalization between blocks then lead to a long-chain molecular wire. Researchers (*150*) have found varying degrees of conductivity in bisaxially coordinated macrocyclic ruthenium complexes $[(Mac)RuL]_n$. For example, when Mac is phthalocyanine and when L is pyrazine or 1,2,4,5-tetraazine, the conductivity was found to be 10^{-7} S cm^{-1} (*151*) and 10^{-1} S cm^{-1} (*152*), respectively.

Other researchers have investigated intramolecular energy and electron transfer in supramolecular species based on ruthenium(II) polypyridine systems (*153*). These supramolecular species could perform the same function as light harvesting structures found in the photosynthetic apparatus.

The potential development of optoelectronic devices based on nonlinear polarization of the MMCT transitions of mixed-valence complexes has been the subject of an investigation (*100*). The hyperpolarizabilities measured for the complexes $[(CN)_5Ru(\mu\text{-}CN)Ru(NH_3)_5]^-$ and $[(\eta^5\text{-}C_5H_5)Ru(PPh_3)_2(\mu\text{-}CN)Ru(NH_3)_5]^{3+}$ are among the largest known for a solution species. The tunability of MMCT energy is an added advantage for the construction of nonlinear optical devices.

III. Electron Exchange

A. Theory

1. Magnetic Electron Exchange

If we consider a system composed of metal A with Spin $\vec{S}_a$ and metal B with spin $\vec{S}_b$, which are bridged by an organic molecule L,

$$M_A\text{—}L\text{—}M_B,$$

then the Hamiltonian for the intramolecular magnetic interaction between spins can be written

$$\mathcal{H} = -2J\vec{S}_a\cdot\vec{S}_b, \tag{35}$$

where the exchange coupling constant J is positive if the spins are parallel and negative if they are paired. In the literature, Eq. (35) can be found with $-J$, $2J$, or J instead of $-2J$ and so the proper conversion should be made when comparing data.

If two metal ions with $\mathbf{S} = \frac{1}{2}$ are antiferromagnetically coupled, a

singlet ground state and an excited triplet state that are separated in energy by $-2J$ are created:

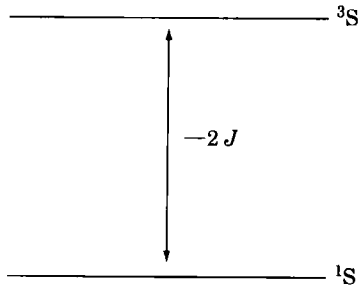

Ferromagnetic coupling results in the formation of a triplet ground state and excited singlet state:

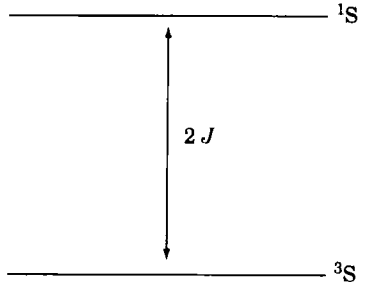

Whether a singlet or triplet ground state is formed depends on the relative magnitude of ferromagnetic (J_F) and antiferromagnetic (J_{AF}) terms,

$$2J = J_F - J_{AF}, \tag{36}$$

where J_F represents the overall spin pairing energy and J_{AF} is the energy released as a result of the coupling of spins (a weak bonding interaction). The value of J_F is usually thought to be small relative to J_{AF}, although *ab initio* calculations of dinuclear Cu(II) complexes with short metal–metal separations have shown J_F to make a significant contribution to the total exchange constant $2J$ (*154*).

2. The Charge Transfer Model for Antiferromagnetic Exchange

The magnitude of J_{AF} has been interpreted by using parameters that reflect the extent of electron exchange stabilization (*155–159*), the

extent of overlap between coupled metal orbitals (*160*), or both. The approach presented in this chapter is developed from the same conceptual basis as that for Marcus electron-transfer theory and the Hush model for intervalence transitions.

The electron-exchange interaction can be described (*155*) as resulting from the mixing of the charge transfer state F with the initial state I,

$$\overset{\uparrow}{M_A}\!-\!L\!-\!\overset{\downarrow}{M_B} \xrightarrow{E'_{op}} M_A\!-\!L\!-\!\overset{\uparrow\downarrow}{M_B} \qquad (37)$$

I $\qquad\qquad$ F

This mixing can occur only if the spins in state I are antiparallel and result in the stabilization energy J_{AF}. The potential energy-configuration diagram representing initial and final states in which E'_0 is not large is shown in Fig. 13. E'_{op} is the charge transfer energy between initial and final states at the same nuclear configuration. H_{ab} is the resonance energy (or tunneling matrix element T_{ab}) between the two states. When E'_0 is large, poor mixing of states and consequently very weak antiferromagnetic exchange result. The analogy between Fig. 13 and the potential energy-configuration diagram (Fig. 1b) for asymmetric mixed-valence complexes should be obvious. However, an important difference is the addition of a spin pairing energy term (*161*), estimated to be approximately 6000 cm^{-1} if Ru(IV) has spin = 0, which will shift E'_{op} to higher energies.

Expressions for the antiferromagnetic exchange term J_{AF} have appeared in the literature (*155–159*). Bertrand (*159*) gives a complete derivation with the final result,

$$J_{AF} = \frac{2|H_{ab}|^2}{E'_{op}}. \qquad (38)$$

This result is an approximation but nevertheless is a valuable guide to the design of exchange coupled systems. More rigorous *ab initio* methods that take into account second-order effects are available (*154*).

The predicted MMCT transition of an antiferromagnetically exchanged coupled system has not been observed experimentally. This may be because bridging ligands that give rise to strong antiferromagnetic coupling will also give rise to an intense ligand-to-metal charge-transfer transition in the visible region (see Section III.A.3), which may overlap and obscure the MMCT transition. If so, electroabsorption spectroscopy may be of some help in deconvoluting LMCT and MMCT

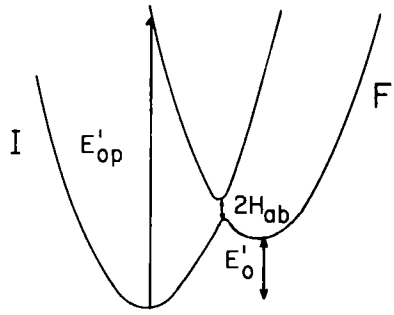

FIG. 13. The potential energy-configuration diagram representing initial *I* and final *F* states.

bands. An antiferromagnetically exchange coupled system will have an MMCT transition band that will be treatable by the Hush model or the MO vibronic coupling model for intervalence transitions. A theoretical study of a delocalized exchange coupled system that uses the vibronic coupling model has appeared in the literature (*162*). It does, however, make the assumption that the ground state is not a singlet.

3. Superexchange

In the discussion so far the nature of the bridging ligand has not been treated and yet it is of paramount importance in determining the magnitude of H_{ab} and hence J_{AF}. For the systems of this chapter, the metal ions are too far apart to interact directly as shown in Eq. (37), and, for metal–metal coupling to occur, bridging ligand orbitals must play an important role. It was Kramers in 1934 (*163*) who proposed that ligand-to-metal charge-transfer LMCT excited states were involved,

$$\uparrow M_A — \uparrow\downarrow L — \downarrow M_B \xrightarrow{E_{lmct}} \uparrow M_A — \downarrow L — \uparrow\downarrow M_B \qquad (39)$$

In the LMCT excited state, the unpaired electrons can couple but can do so only if their spins are opposite. The mixing of the LMCT excited state with the ground state therefore stabilizes a ground state in which the electrons are antiparallel. This ligand mediated electron exchange mechanism is called superexchange and is analogous to the hole-transfer superexchange mechanism discussed in Section II.B.2.b.

The optimization of superexchange in Eq. (39) requires that the magnetic orbitals (orbitals containing one electron) overlap simultaneously with a single ligand molecular orbital, the superexchange pathway.

To overlap effectively, magnetic orbitals must have the same symmetry and be as close in energy as possible to the ligand molecular orbital. The interaction will result in an LMCT transition whose energy is a measure of the gap between magnetic orbitals and the superexchange pathway (*78*) and whose oscillator strength is a measure of the electronic interaction (*164–166*).

4. Experimental Evaluation of the Electron Exchange Constant J

The magnetic properties of a compound are evaluated by measuring its magnetic susceptibility, χ, as a function of temperature (*167*). For an antiferromagnetically coupled dimer complex, the molar magnetic susceptibility is determined by the thermal population distribution of singlet ground and triplet excited states and is usually given by the modified Bleaney–Bowers expression (*168*),

$$\chi_m = \frac{C}{(T-\theta)} + \left(\frac{2N\bar{g}^2\beta^2}{3kT}\right)\left[1 + \left(\frac{1}{3}\right)\exp\left(\frac{-2J}{kT}\right)\right]^{-1} + \chi_p, \qquad (40)$$

where $\bar{g}$ is the powder average g value, $C/(T-\theta)$ is a Curie–Weiss term that corrects for any paramagnetic impurity at low temperatures, and χ_p is a correction for any background paramagnetism. The treatment of the temperature dependence of magnetic susceptibility is almost completely dominated by spin, but for Ru(III), orbital angular momentum may make a significant contribution. Drillon and Georges (*169*) have developed procedures for including the orbital contribution for $t_{2g}{}^n$ configurations, but analytical expressions are not available. A good estimate of the electron exchange constant J for Ru(III) dimers can be had by assuming isotopically coupled, $S = \frac{1}{2}$ spins and by using Eq. (40).

B. Studies of Exchange Coupled Dinuclear Ruthenium Complexes

There have been only a handful of studies on exchange coupled ruthenium dimers and yet the information available on metal–metal coupling is potentially as valuable as that obtained from mixed-valence complexes. The reason for this lack of activity has been the greater familiarity of researchers with the chemistry of Ru(II) bound to π-acid ligands. The synthetic pathways to complexes of this type are well explored (*7*) and possess the tremendous advantages of stability and ease of handling. Ru(II) complexes that incorporate anionic π donor

ligands are unstable with respect to ligand substitution and this lack of complex integrity is an extreme practical disadvantage. On the other hand, Ru(III) complexes that incorporate π-donor ligands are quite stable, and so the synthesis of stable Ru(III) dinuclear complexes that have π-donor bridging ligands needs only the development of synthetic pathways to become easily accessible for study.

The first attempt to study electron exchange in dinuclear Ru(III) complexes produced a negative result. Complexes of the type $[\{(bpy)Ru(Cl)\}_2(\mu\text{-L})]^{6+}$, where L is the π accepting ligands pyrazine, 4,4′-bipyridine and 1,2-bis(4-pyridyl)ethane, showed little if any evidence for magnetic interactions down to liquid-helium temperatures (*169*). This led the researchers to suggest that the primary orbital mechanism for metal–metal coupling in the mixed-valence analogues is by $d\pi$Ru(II)-π^*(L) mixing (electron transfer superexchange) because oxidation leads to orbital contraction of the $d\pi$ orbitals and to their stabilization relative to the LUMO of the bridging ligand. Electron exchange is extremely weak in these complexes because of the large difference in energy between the Ru(III) $d\pi$ orbitals and either the π symmetry LUMO or HOMO of the bridging ligand. These same arguments could explain the weak antiferromagnetic coupling ($2J = -6$ cm^{-1}) that was seen for the fully oxidized Creutz–Taube ion $[\{(NH_3)_5Ru\}_2(\mu\text{-pyz})]^{6+}$ (*59, 170*), and together these results serve to emphasize the unsuitability of π acceptor bridging ligands as a medium for electron exchange in Ru(III)–Ru(III) dinuclear complexes.

The first real indication of antiferromagnetic superexchange in ruthenium dimers that possessed polyatomic bridging ligands was found for the complex $[\{(NH_3)_5Ru\}_2(\mu\text{-}t\text{-BuMN})]^{5+}$ (*76*), where

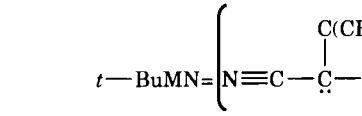

The magnetic susceptibility of this complex (0.98 μ_B) is severely depressed relative to those of mononuclear low-spin Ru(III) complexes, which range from 1.9 to 2.07 μ_B (*171*). Unfortunately, the temperature dependence of the magnetic susceptibility of this complex and other derivatives was not tested for and so a measure of antiferromagnetic J is not available. The lone electron pair of the bridging ligand's central carbon can delocalize into the π systems of both nitrile groups. This provides a superexchange pathway of π symmetry that spans the entire molecule and can interact simultaneously with both metal ions. It is

not unexpected that the mixed-valence complex also shows evidence of strong metal–metal coupling and is a delocalized class III system.

The possibility that long-range antiferromagnetic coupling might occur between magnetic orbitals bridged by an easily polarizable, extended π HOMO system led researchers to prepare (*78*) the dinuclear Ru(III) complexes $[\{(NH_3)_5Ru\}_2(\mu\text{-L})]^{4+}$, where L is $Dicyd^{2-}$, Me_2-$Dicyd^{2-}$, Cl_2Dicyd^{2-}, and Cl_4Dicyd^{2-}. The temperature dependence of magnetic susceptibility showed the complexes to be antiferromagnetically coupled systems, as is illustrated in Fig. 14. The best fits of the magnetic data gave values of $-J$ for the complexes, which varied from a low of -61.9 to $\geq 400\ cm^{-1}$. Antiferromagnetic coupling of this magnitude at an estimated through-space separation between metal ions of 13.2 Å was unprecedented for any metal ion dimer system (*78, 173*) and was shown to be due to a continuous and energetically favorable superexchange pathway involving the magnetic $d\pi$ orbitals of the Ru(III) ions and the π HOMO of the bridging $Dicyd^{2-}$ ligand. The details of this study deserve further mention.

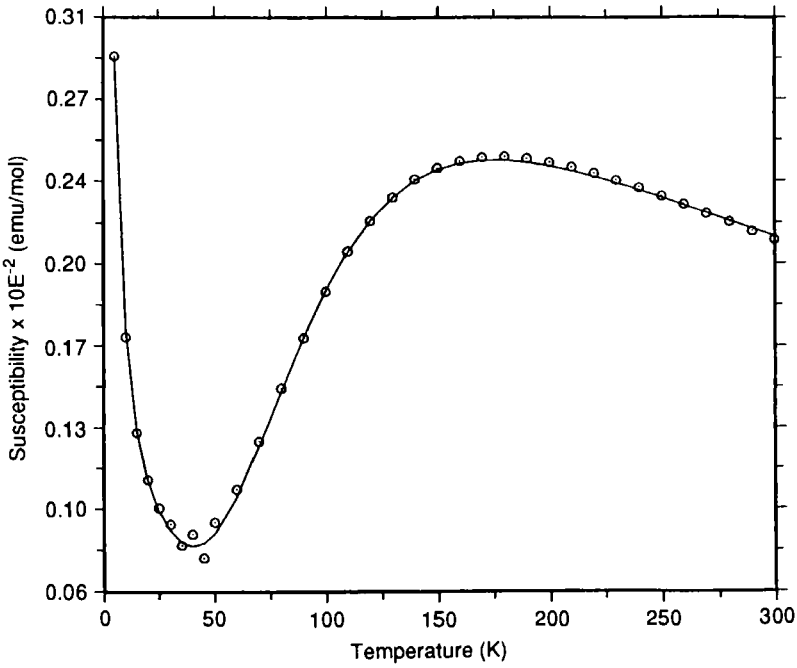

FIG. 14. Experimental (⊙) and modeled (—) by using Eq. (40) temperature dependencies of the molar magnetic susceptibility of $[\{(NH_3)Ru\}_2(\mu\text{-Dicyd})][OTs]_4$. [Reproduced with permission from Ref. (*78*). Copyright (1992) American Chemical Society.]

Extended Huckel calculations were performed using the crystal structure data (*174*) of the free dianion ligands. The frontier orbitals of the Dicyd^{2-} are illustrated in Fig. 15 and show that both HOMO and SHOMO are of π symmetry and span the entire molecule. A crystal structure determination of the complex [{$(NH_3)Ru$}$_2$(μ-Dicyd)][OTs]$_4$

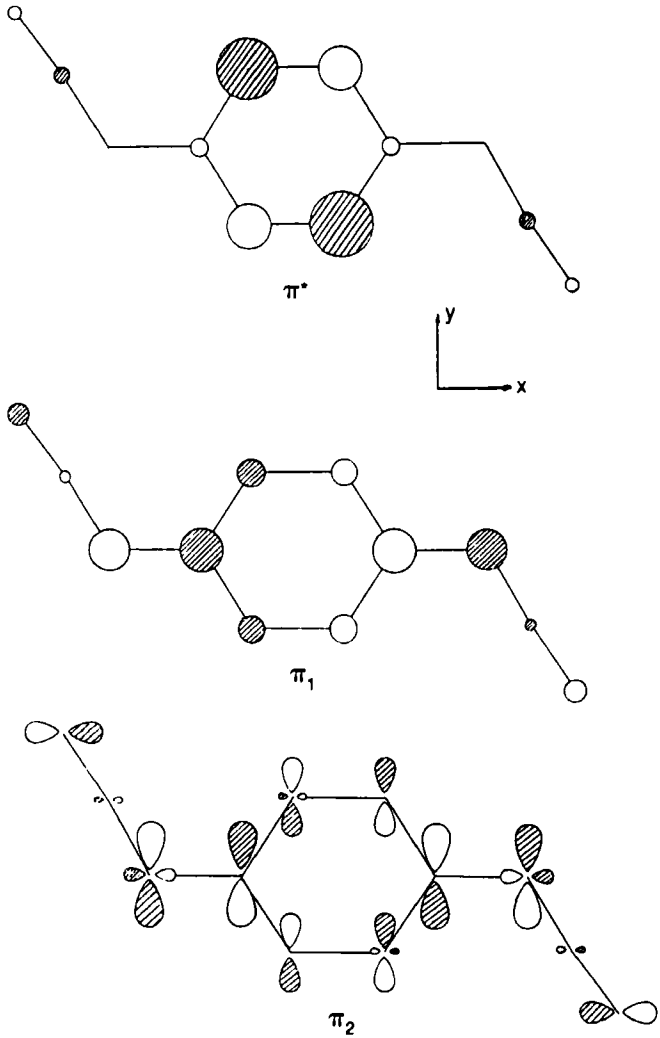

FIG. 15. Frontier orbitals of Dicyd^{2-} from EHMO calculations. Minor orbital corrections are omitted for clarity. [Reproduced with permission from Ref. (*78*). Copyright (1992) American Chemical Society.]

(where OTs is tosylate anion) was also done and showed that planarity of the bridging ligand was retained upon coordination. However, two conformations of the dinuclear complex were observed. For conformer A, both Ru(III)–cyanamide bonds are essentially linear and, for conformer B, both Ru(III)–cyanamide bonds are bent. Because of the different Ru–NCN bond angles, both HOMO and SHOMO are potential superexchange pathways. The energy gap between magnetic orbitals and the HOMO of the $Dicyd^{2-}$ derivatives was estimated from the energy of the LMCT band associated with the Ru(III)–cyanamide chromophore for the complexes in aqueous solution. After a correction to compensate for the change in inner and outer coordination sphere configurations resulting from a transition into an excited vibrational level of the excited LMCT state, the energy gaps between magnetic orbitals and the superexchange pathway were estimated at 0.48, 0.63, 0.74, and 0.94 eV for $[\{(NH_3)_5Ru\}_2(\mu\text{-L})]^{4+}$, where L is Me_2Dicyd^{2-}, $Dicyd^{2-}$, Cl_2Dicyd^{2-}, and Cl_4Dicyd^{2-}, respectively. Qualitatively, the trend in the value of $-J$ increased with decreasing energy gap as expected. The complex with the smallest energy gap, $[\{(NH_3)_5Ru\}_2(\mu\text{-}Me_2Dicyd)]^{4+}$, is diamagnetic at room temperature and only a lower limit of $-J \geq 400\ cm^{-1}$ could be estimated.

The effect of $Dicyd^{2-}$ ligand planarity on the magnitude of superexchange was illustrated by the study (*175*) of the complex $[\{(NH_3)_5Ru\}_2(\mu\text{-}Me_4Dicyd)]^{4+}$. Temperature-dependent magnetic susceptibility data gave, after modeling with Eq. (40), $-J = 110\ cm^{-1}$. For the Me_4Dicyd^{2-} ligand, steric repulsion forces the cyanamide groups into an anticonfiguration out of the phenyl ring plane. An EHMO calculation of the ligand showed a HOMO with electron density mostly localized on the phenyl ring. This would result in poor overlap with the magnetic orbitals and a reduction in superexchange compared with the planar $Dicyd^{2-}$ derivatives. For the complex $[\{(NH_3)_5Ru\}_2(\mu\text{-}Me_4Dicyd)]^{4+}$, the energy gap between magnetic orbitals and the superexchange pathway can be estimated at 0.76 eV. This value is very close to that of $[\{(NH_3)_5Ru\}_2(\mu\text{-}Cl_2Dicyd)]^{4+}$, for which $-J = 95.9\ cm^{-1}$, and suggests that the energy gap between magnetic orbitals and $Dicyd^{2-}$ orbitals may be the most important factor in determining the magnitude of $-J$.

The complex $[\{(NH_3)_5Ru\}_2(\mu\text{-Dicyd})]^{4+}$ showed an interesting dependence of $-J$ on the counteranion (*78*). When the counterion was ClO_4^-, the complex was nearly diamagnetic at room temperature, with an estimated $-J \leq 400\ cm^{-1}$. When the counterion was OTs^-, $-J = 100\ cm^{-1}$. Counterion effects are usually ascribed to intermolecular exchange interactions. However, in this case, $|\Delta J| \approx 300\ cm^{-1}$ is far too large to be explained by relatively weak intermolecular interactions

between octahedral Ru(III) ions (*168, 171*). The solvent-dependent metal–metal coupling that was seen for mixed-valence complexes (discussed in Section II.C.2.c) may have an application here. It is suggested that hydrogen bonding interactions in the crystal lattice between counterions and solvent molecules with ammines bonded to Ru(III) can help decouple the Ru(III) ion from the bridging ligand (*165, 166*). Solvent-dependent antiferromagnetic exchange was indicated by the observation that $[\{(NH_3)_5Ru\}_2(\mu\text{-}Me_2Dicyd)]^{4+}$ forms diamagnetic solutions in nitromethane, whereas those of dimethyl sulfoxide are paramagnetic (*176*). The solution ^1H NMR spectra show that complex integrity is maintained in both solvents.

Attempts to see an MMCT band for the Ru(III)–Ru(III) dinuclear complexes were unsuccessful (*78, 79*). The intense low-energy LMCT bands are likely to obscur these transitions. The values of H_{ab} for the complexes $[\{(NH_3)_5Ru\}_2(\mu\text{-}L)]^{4+}$ were estimated from Eq. (38) and compared with H_{ad} calculated for the mixed-valence complexes using Eq. (15). H_{ab} was significantly larger than H_{ad} and it was suggested that solid-state geometry was optimal for metal–metal coupling. Metal–metal coupling in the mixed-valence complexes is also attenuated by strong solvent donor interactions with the ammine ligands (*176*) and this may partially account for the difference between H_{ab} and H_{ad}. This is not to say that H_{ab} and H_{ad} should be equivalent because they are derived from different state descriptions.

IV. Future Studies

Electroabsorption spectroscopy and its application to MMCT transitions (*17, 18, 104*) are important developments that will test current theories and increase our understanding of the factors that control superexchange phenomena. It is to be hoped that the use of electroabsorption spectroscopy becomes commonplace.

Selective perturbation of metal–metal coupling by either inner-sphere or outer-sphere manipulations will continue. Aside from increasing our understanding of metal–metal superexchange coupling, these studies will probe the nature of solvent–solute interactions and perhaps be applicable to the design of molecular devices. The synthesis of novel nonlinear optical materials that incorporate mixed-valence metal systems will be the subject of much interest (*100*).

There are very few examples of exchange coupled dinuclear ruthenium complexes and a clear opportunity exists for further study. All dinuclear complexes that possess anionic bridging ligands (*76, 81–85,*

88, 91, 92, 95, 141) and can form stable Ru(III)–Ru(III) complexes should be evaluated for antiferromagnetic exchange. More results are needed to elucidate the dependence of electron exchange on the relative symmetry and energy of the superexchange pathway. The distance dependence of electron exchange poses interesting questions. A fully delocalized system should have very little distance dependence. The synthesis of $[\{(NH_3)_5Ru\}_2(\mu\text{-Dicyd})]^{4+}$ complexes and the observation of strong antiferromagnetic coupling between metal ions separated by 13 Å are a consequence of the very special properties of the bridging $Dicyd^{2-}$ ligand. The $Dicyd^{2-}$ molecule is easily oxidized, is highly polarizable, and possesses a π HOMO that spans the entire molecule. Novel bridging ligands with similar properties should be synthesized.

Ondrechen *et al.* (*177, 178*) have explored the design of conductive mixed valency oligomers. The polarizability of the bridging ligand had a direct impact on both spectroscopic and conductive properties. What is now needed is the practical application of superexchange phenomena to the synthesis of novel solid-state materials.

V. Glossary of Abbreviations and Ligand Structures

azpy

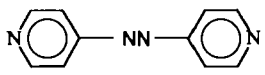

bphy

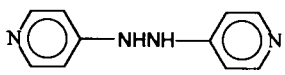

abpy

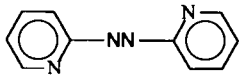

bpt $^-$

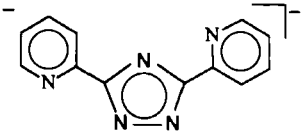

adc $^{2-}$

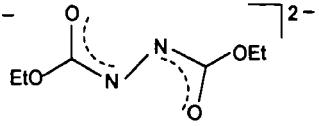

bpzt$^-$

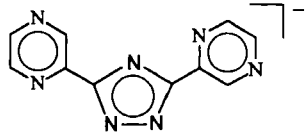

bptz

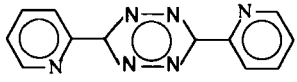

BiBzIMH$_2$

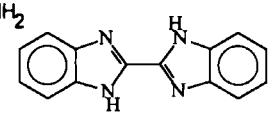

mbpt $^-$

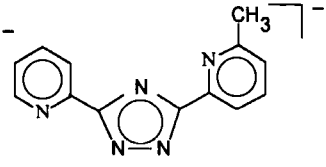

BilMH$_2$

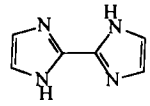

bpm

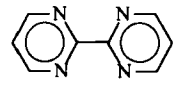

bpbimH$_2$

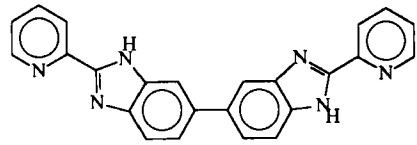

bpy

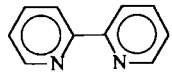

bppz

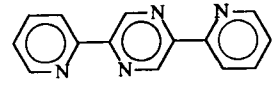

Me$_2$bpy

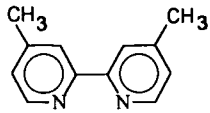

dtdp

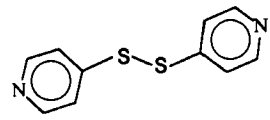

(COOEt)$_2$bpy

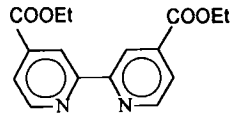

dpb

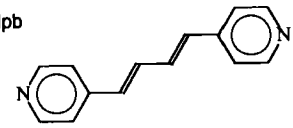

4,4'-bpy

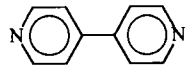

dph

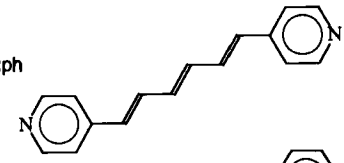

4cp

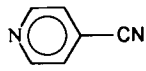

dpo

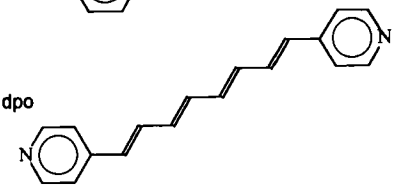

3cp

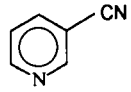

chd^{2-}

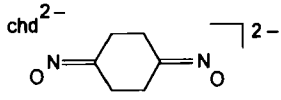

dpimbH$_2$

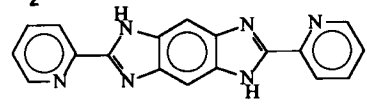

3-dpph

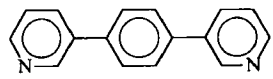

dpph

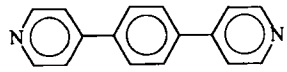

dpdph

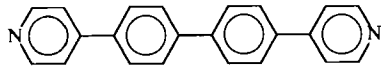

dts

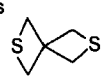

dtsd

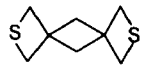

dtst

dcpy^{2-}

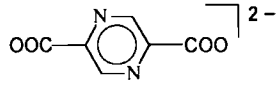

15dcn

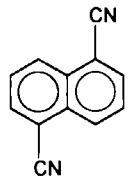

16dcn

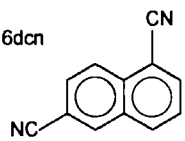

12dcb

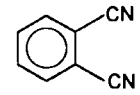

13dcb

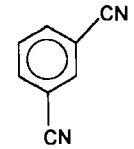

14dcb

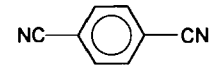

dpmn

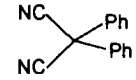

dcyH

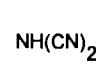

13dca

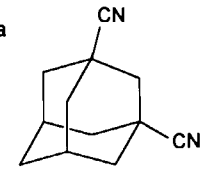

dicyd^{2-}

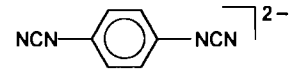

Me_2dicyd^{2-}

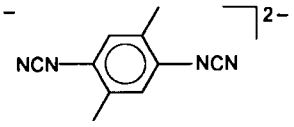

17dcn

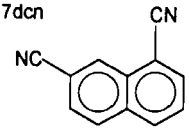

26dcn

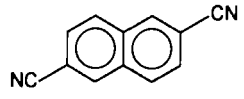

dto

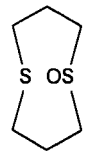

dpp

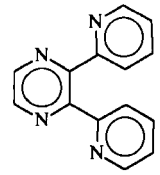

dpq

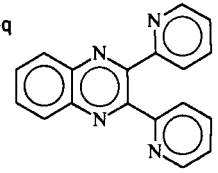

fum

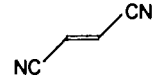

isn

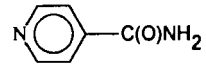

Me_4dicyd^{2-}

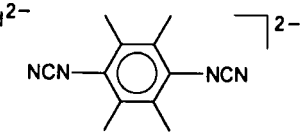

Cl_2dicyd^{2-}

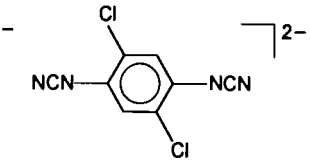

Cl_4dicyd^{2-}

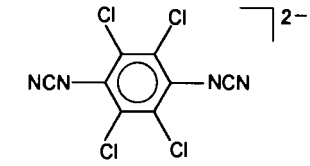

pym

$pyzc^-$

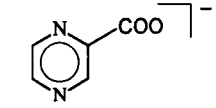

phen

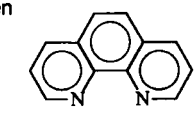

NO_2phen

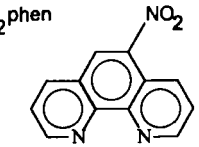

py

Me_2phen

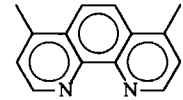

Me_4phen

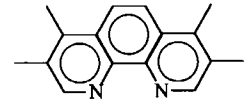

pyz

ppdcp

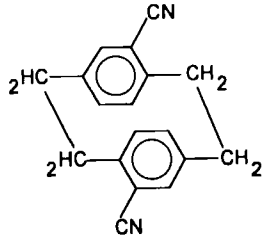

tptp

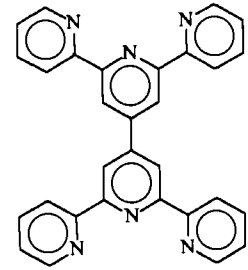

tppz

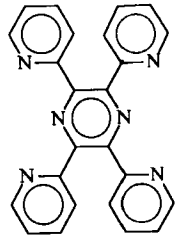

$tpbpH_2$

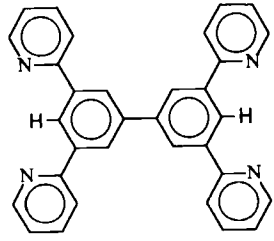

tppt

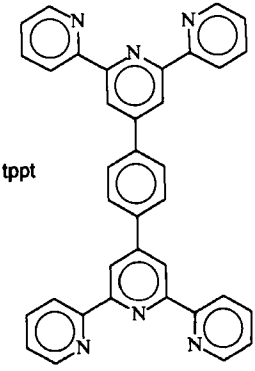

terpy

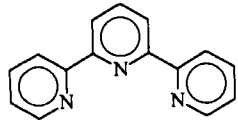

tterpy

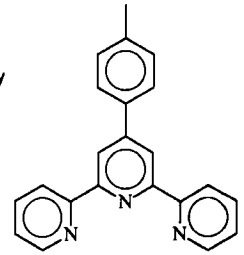

tpdptp

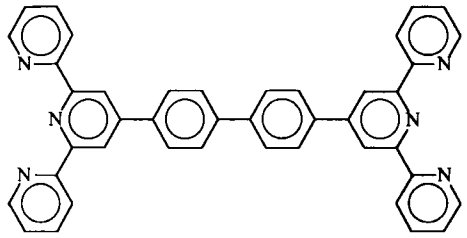

ACKNOWLEDGMENTS

The financial support of NSERC (Canada) and Carleton University is gratefully acknowledged. I would also like to thank NSERC (Canada) for the award of a University Research Fellowship and Johnson-Matthey P.L.C. for the loan of ruthenium trichloride hydrate in support of my research program.

REFERENCES

1. Seddon, E. A., and Seddon, K. R., "The Chemistry of Ruthenium," 2nd ed. Elsevier, Amsterdam, 1984.
2. Allen, G. C., and Hush, N. S., *Prog. Inorg. Chem.* **8,** 357 (1967).
3. Robin, M. B., and Day, P., *Adv. Inorg. Chem. Radiochem.* **10,** 247 (1967).
4. (a) Hush, N. S., *Prog. Inorg. Chem.* **8,** 391 (1967); (b) Hush, N. S., *Trans. Faraday Soc.* **57,** 557 (1961); (c) Hush, N. S., *Electrochim. Acta* **13,** 1005 (1968).
5. Marcus, R. A., *J. Chem. Phys.* **24,** 966 (1956).
6. Marcus, R. A., *J. Chem. Phys.* **26,** 867 (1957); 872 (1957).
7. Creutz, C., *Prog. Inorg. Chem.* **30,** 1 (1983).
8. Meyer, T. J., *Prog. Inorg. Chem.* **30,** 389 (1983).
9. Sutin, N., *Prog. Inorg. Chem.* **30,** 441 (1983).
10. Newton, M. D., *Chem. Rev.* **91,** 767 (1991).

11. Mataga, N., and Kubota, T., "Molecular Interactions and Electronic Spectra." Dekker, New York, 1970.
12. Murrell, J. N., *Quart. Rev. (London)* **15,** 191 (1961).
13. Chen, P., Curry, M., and Meyer, T. J., *Inorg. Chem.* **28,** 2271 (1989).
14. Creutz, C., *Inorg. Chem.* **17,** 3723 (1978).
15. Hupp, J. T., and Meyer, T. J., *Inorg. Chem.* **26,** 2332 (1986).
16. Kober, E. M., Goldsby, K. A., Narayana, D. N. S., and Meyer, T. J., *J. Am. Chem. Soc.* **105,** 4303 (1985).
17. Oh, D. H., and Boxer, S. G., *J. Am. Chem. Soc.* **111,** 1130 (1989).
18. Oh, D. H., Sano, M., and Boxer, S. G., *J. Am. Chem. Soc.* **113,** 6880 (1991).
19. Marcus, R. A., *J. Chem. Phys.* **43,** 679 (1965).
20. Cannon, R. D., *Chem. Phys. Lett.* **49,** 299 (1977).
21. Brunschwig, B. S., Ehrenson, S., and Sutin, N., *J. Phys. Chem.* **90,** 3657 (1986).
22. Sutton, J. E., and Taube, H., *Inorg. Chem.* **20,** 3125 (1981).
23. Reimers, J. R., and Hush, N. S., *Inorg. Chem.* **29,** 3686 (1990); 4510 (1990).
24. (a) Piepho, S. B., Krausz, E. R., and Schatz, P. N., *J. Am. Chem. Soc.* **100,** 2996 (1978); (b) Wong, K. Y., and Schatz, P. N., *Prog. Inorg. Chem.* **28,** 369 (1981).
25. Buhks, E., Ph.D. Thesis, Tel Aviv University, Tel Aviv, 1980.
26. Wong, K. Y., and Schatz, P. N., *in* "Mechanistic Aspects of Inorganic Reactions" (Rorabacher, D. B., and Endicott, J. F., Eds.), Chap. 12, p. 281. American Chemical Society, Washington, D.C., 1982.
27. (a) Hush, N. S., *in* "Mechanistic Aspects of Inorganic Reactions" (Rorabacher, D. B., and Endicott, J. F., Eds.), Chap. 13, p. 301. American Chemical Society, Washington, D.C., 1982; (b) p. 330. American Chemical Society, Washington, D.C., 1982.
28. Hush, N. S., *in* "Mixed-Valence Compounds" (Brown, D. B., Ed.), p. 151. D. Reidel, Dordrecht, Holland, 1980.
29. Ko, J., and Ondrechen, M. J., *J. Am. Chem. Soc.* **107,** 6161 (1985).
30. Dubicki, L., Ferguson, J., and Krausz, E. R., *J. Am. Chem. Soc.* **107,** 179 (1985).
31. (a) Root, L. J., and Ondrechen, M. J., *Chem. Phys. Lett.* **93,** 421 (1982); (b) Ondrechen, M. J., Ko, J., and Root, L., *J. Phys. Chem.* **88,** 5919 (1984); (c) Ko, J., and Ondrechen, M. J., *Chem. Phys. Lett.* **112,** 507 (1984); (d) Ko, J., Zhang, L.-T., and Ondrechen, M. J., *J. Am. Chem. Soc.* **108,** 1712 (1986); (e) Zhang, L.-T., Ko, J., and Ondrechen, M. J., *J. Am. Chem. Soc.* **109,** 1666 (1987); (f) Ondrechen, M. J., Ko, J., and Zhang, L.-T., *J. Am. Chem. Soc.* **109,** 1672 (1987); (g) Zhang, L.-T., Ko, J., and Ondrechen, M. J., *J. Phys. Chem.* **93,** 3030 (1989).
32. (a) Piepho, S., *J. Am. Chem. Chem. Soc.* **110,** 6319 (1988); (b) Piepho, S. B., *in* "Mixed-Valency Systems: Applications in Chemistry, Physics and Biology" (Prassides, K., Ed.), p. 329. Kluwer Academic, Dordrecht, 1991; (c) Schatz, P. N., *in* "Mixed-Valency Systems: Applications in Chemistry, Physics and Biology" (Prassides, K., Ed.), p. 7. (d) Riley, M. J., and Krausz, E. R., *in* "Mixed-Valency Systems: Applications in Chemistry, Physics and Biology" (Prassides, K., Ed.), p. 341.
33. Piepho, S., *J. Am. Chem. Chem. Soc.* **112,** 4197 (1990).
34. Salaymeh, F., Berhane, S., Yusof, R., de la Rosa, R., Fung, E. Y., Matamoros, R., Lau, K. W., Zheng, Q., Kober, E. M., and Curtis, J. C., *Inorg. Chem.* **32,** 3895 (1993).
35. Johnson, J. E. B., de Groff, C., and Ruminski, R. R., *Inorg. Chim. Acta* **187,** 73 (1991).
36. Poppe, J., Moscherosch, M., and Kaim, W., *Inorg. Chem.* **32,** 2640 (1993).
37. Ernst, S., Kasack, V., and Kaim, W., *Inorg. Chem.* **27,** 1146 (1988).
38. Kaim, W., Kasack, V., Binder, H., Roth, E., and Jordanov, J., *Angew. Chem. Int. Ed. Engl.* **27,** 1174 (1988).

39. Bardwell, D., Jeffery, J. C., Joulié, L., and Ward, M. D., *J. Chem. Soc. Dalton Trans.*, 2255 (1993).
40. de Sousa Moreira, I., and Franco, D. W., *J. Chem. Soc. Chem. Commun.*, 450 (1992).
41. Ruminski, R. R., Cockroft, T., and Shoup, M., *Inorg. Chem.* **27,** 4026 (1988).
42. Beley, M., Collin, J.-P., Louis, R., Metz, B., and Sauvage, J.-P., *J. Am. Chem. Soc.* **113,** 8521 (1991).
43. Collin, J.-P., Lainé, R., Launay, J.-P., Sauvage, J.-P., and Sour, A., *J. Chem. Soc. Chem. Commun.*, 434 (1993).
44. Palaniappan, V., Yadav, S. K. S., and Agarwala, U. C., *Polyhedron.* **4,** 1457 (1985).
45. de la Rosa, R., Chang, P. J., Salaymeh, F., and Curtis, J. C., *Inorg. Chem.* **24,** 4229 (1985).
46. Salaymeh, F., Berhane, S., Yusof, R., de la Rosa, R., Fung, E. Y., Matamoros, R., Lau, K. W., Zheng, Q., Kober, E. M., and Curtis, J. C., *Inorg. Chem.* **32,** 3895 (1993).
47. Brant, P., and Stephenson, T. A., *Inorg. Chem.* **26,** 22 (1987).
48. Hush, N. S., *Chem. Phys.* **10,** 361 (1975).
49. Larsson, S., *J. Am. Chem. Soc.* **103,** 4034 (1981).
50. Kosloff, R., and Ratner, M. A., *Israel J. Chem.* **30,** 45 (1990).
51. Broo, A., and Larsson, S., *Chem. Phys.* **161,** 363 (1992).
52. Kaim, W., and Kasack, V., *Inorg. Chem.* **29,** 4696 (1990).
53. Cooper, J. B., MacQueen, D. B., Petersen, J. D., and Wertz, D. W., *Inorg. Chem.* **29,** 3701 (1990).
54. Matsubara, T., and Ford, P. C., *Inorg. Chem.* **15,** 1107 (1976).
55. Szentrimay, R., Yeh, P., and Kuwana, T., *in* "Electrochemical Studies of Biological Systems" (Sawyer, D. T., Ed.). American Chemical Society, Washington, D.C., 1977.
56. Dong, Y., Hupp, J. T., and Yoon, D. I., *J. Am. Chem. Soc.* **115,** 4379 (1993).
57. Roberts, J. A., and Hupp, J. T., *Inorg. Chem.* **31,** 160 (1992).
58. Krausz, E., Burton, C., and Broomhead, J., *Inorg. Chem.* **20,** 434 (1981).
59. Furholz, U., Burgi, H.-B., Wagner, F. E., Stebler, A., Ammeter, J. H., Krausz, E., Clark, R. J. H., Stead, M. J., and Ludi, A., *J. Am. Chem. Soc.* **106,** 121 (1984).
60. Stebler, A., Ammeter, J. H., Furholz, U., and Ludi, A., *Inorg. Chem.* **23,** 2764 (1984).
61. Furholz, U., Stefan, J., Burgi, H.-B., and Ludi, A., *Inorg. Chem.* **24,** 943 (1985).
62. Krausz, E. R., and Mau, A. W. H., *Inorg. Chem.* **25,** 1484 (1986).
63. Krausz, E., and Ludi, A., *Inorg. Chem.* **24,** 939 (1985).
64. Creutz, C., and Chou, M. H., *Inorg. Chem.* **26,** 2995 (1987).
65. Joss, S., Hasselbach, K. M., Burgi, H.-B., Wordel, R., Wagner, F. E., and Ludi, A., *Inorg. Chem.* **28,** 1815 (1989).
66. Best, S. P., Clark, R. J. H., McQueen, R. C. S., and Joss, S., *J. Am. Chem. Soc.* **111,** 548 (1989).
67. Piepho, S. B., Krausz, E. R., and Schatz, P. N., *Chem. Phys. Lett.* **55,** 539 (1978).
68. Woitellier, S., Launay, J. P., and Spangler, C. W., *Inorg. Chem.* **28,** 758 (1989).
69. Kim, Y., and Lieber, C. M., *Inorg. Chem.* **28,** 3990 (1989).
70. Launay, J.-P., Tourrel-Paagis, M., Libskier, J.-F., Marvaud, V., and Joachim, C., *Inorg. Chem.* **30,** 1033 (1991).
71. Stein, C. A., and Taube, H., *J. Am. Chem. Soc.* **103,** 693 (1981).
72. Stein, C. A., Lewis, N. A., and Steitz, G., *J. Am. Chem. Soc.* **104,** 2596 (1982).
73. Sedney, D., and Ludi, A., *Inorg. Chim. Acta* **47,** 153 (1981).
74. Amer, S. I., Dasgupta, T. P., and Henry, P. M., *Inorg. Chem.* **22,** 1970 (1983).
75. Sutton, J. E., Krentzien, H., and Taube, H., *Inorg. Chem.* **21,** 2842 (1982).

76. Krentzien, H., and Taube, H., *Inorg. Chem.* **21,** 4001 (1982).
77. Richardson, D. E., and Taube, H., *J. Am. Chem. Soc.* **105,** 40 (1983).
78. Aquino, M. A. S., Lee, F. L., Gabe, E. J., Bensimon, C., Greedan, J. E., and Crutchley, R. J., *J. Am. Chem. Soc.* **114,** 5130 (1992).
79. Aquino, M. A. S., Bostock, A. E., and Crutchley, R. J., *Inorg. Chem.* **29,** 3641 (1990).
80. Sano, M., and Taube, H., *J. Am. Chem. Soc.* **113,** 2327 (1991).
81. Hage, R., Haasnoot, J. G., Reedijk, J., Wang, R., and Vos, J. G., *Inorg. Chem.* **30,** 3263 (1991).
82. Haga, M., Matsumura-Inoue, T., and Yamabe, S., *Inorg. Chem.* **26,** 4148 (1987).
83. Haga, M., and Bond, A. M., *Inorg. Chem.* **30,** 475 (1991).
84. Rillema, D. P., Sahai, R., Mathews, P., Edwards, A. K., Shaver, R. J., and Morgan, L., *Inorg. Chem.* **29,** 167 (1990).
85. Haga, M., Ano, T., Kano, K., and Yamabe, S., *Inorg. Chem.* **30,** 3843 (1991).
86. Goldsby, K. A., and Meyer, T. J., *Inorg. Chem.* **23,** 3002 (1984).
87. Wallace, A. W., Murphy, W. R., and Petersen, J. D., *Inorg. Chim. Acta* **166,** 47 (1989).
88. Ohno, T., Nozaki, K., and Haga, M., *Inorg. Chem.* **31,** 4256 (1992).
89. Geno, M. J. K., and Dawson, J. H., *Inorg. Chem.* **23,** 1182 (1984).
90. Cloninger, K. K., and Callahan, R. W., *Inorg. Chem.* **20,** 1611 (1981).
91. Palaniappan, V., and Agarwala, U. C., *Inorg. Chem.* **27,** 3568 (1988).
92. Palaniappan, V., Sathaiah, S., Bist, H. D., and Agarwala, U. C., *J. Am. Chem. Soc.* **110,** 6403 (1988).
93. Das, B. K., and Chakravarty, A. R., *Inorg. Chem.* **30,** 4978 (1991).
94. Chang, J. P., Fung, E. Y., and Curtis, J. C., *Inorg. Chem.* **25,** 4233 (1986).
95. Chou, M. H., Creutz, C., and Sutin, N., *Inorg. Chem.* **31,** 2318 (1992).
96. Fagalde, F., and Katz, N. E., *J. Chem. Soc. Dalton Trans.*, 571 (1993).
97. (a) Bignozzi, C. A., Paradisi, C., Roffia, S., and Scandola, F., *Inorg. Chem.* **27,** 408 (1988); (b) Roffia, S., Paradisi, C., and Bignozzi, C. A., *J. Electroanal. Chem.* **200,** 105 (1986); (c) Bignozzi, C. A., Roffia, S., and Scandola, F. J., *J. Am. Chem. Soc.* **107,** 1644 (1985).
98. Siddiqui, S., Henderson, W. W., and Shepherd, R. E., *Inorg. Chem.* **26,** 3101 (1987).
99. (a) Vogler, A., and Kisslinger, J., *J. Am. Chem. Soc.* **104,** 2311 (1982); (b) Ludi, A., *Chimia* **26,** 647 (1972).
100. Laidlaw, W. M., Denning, R. G., Verbiest, T., Chauchard, E., and Persoons, A., *Nature* **363,** 58 (1993).
101. Ismail, K. Z., Tunuli, M. S., and Weber, S. G., *Inorg. Chem.* **26,** 1555 (1987).
102. Henderson, W. W., and Shepherd, R. E., *Inorg. Chem.* **24,** 2398 (1985).
103. Curtis, J. C., and Meyer, T. J., *Inorg. Chem.* **21,** 1562 (1982).
104. Reimers, J. R., and Hush, N. S., *in* "Mixed-Valency Systems: Applications in Chemistry, Physics and Biology" (Prassides, K., Ed.), p. 29. Kluwer Academic, Dordrecht, 1991.
105. Sutton, J. E., Sutton, P. M., and Taube, H., *Inorg. Chem.* **18,** 1017 (1979).
106. Hupp, J. T., Dong, Y., Blackbourn, R. L., and Lu, H., *J. Phys. Chem.* **97,** 3278 (1993).
107. Doorn, S. K., and Hupp, J. T., *J. Am. Chem. Soc.* **111,** 1142 (1989).
108. Doorn, S. K., Hupp, J. T., Porterfield, D. R., Campion, A., and Chase, D. B., *J. Am. Chem. Soc.* **112,** 4999 (1990).
109. Bignozzi, C. A., Argazzi, R., Schoonover, J. R., Dyer, R. B., and Scandola, F., *Inorg. Chem.* **31,** 5260 (1992).
110. Cooper, J. B., Vess, T. M., Kalsbeck, W. A., and Wertz, D. W., *Inorg. Chem.* **30,** 2286 (1991).

111. Kober, E. M., Goldsby, K. A., Narayana, D. N. S., and Meyer, T. J., *J. Am. Chem. Soc.* **105,** 4303 (1985).
112. Hupp, J. T., and Meyer, T. J., *Inorg. Chem.* **26,** 2332 (1987).
113. Brunschwig, B. S., Ehrenson, S., and Sutin, N., *J. Phys. Chem.* **90,** 3657 (1986).
114. Kornyshev, A. A., and Ulstrup, J., *Chem. Phys. Lett.* **126,** 74 (1986).
115. Ulstrup, J., *J. Phys. Chem.* **91,** 5153 (1987).
116. (a) Hammack, W. S., Drickamer, H. G., Lowery, M. D., and Hendrickson, D. N., *Chem. Phys. Lett.* **132,** 231 (1986); (b) Lowery, M. D., Hammack, W. S., Drickamer, H. G., and Hendrickson, D. N., *J. Am. Chem. Soc.* **109,** 8019 (1987); (c) Hammack, W. S., Drickamer, H. G., Lowery, M. D., and Hendrickson, D. N., *Inorg. Chem.* **27,** 1307 (1988).
117. (a) Lewis, N. A., and Obeng, Y. S., *J. Am. Chem. Soc.* **110,** 2306 (1988); (b) Lewis, N. A., Obeng, Y. S., and Purcell, W. L., *Inorg. Chem.* **28,** 3796 (1989).
118. (a) Blackbourn, R. L., and Hupp, J. T., *Chem. Phys. Lett.* **150,** 399 (1988); (b) Blackbourn, R. L., and Hupp, J. T., *J. Phys. Chem.* **94,** 1790 (1990).
119. Lewis, N. A., Obeng, Y. S., Taveras, D. V., and van Eldik, R., *J. Am. Chem. Soc.* **111,** 924 (1989).
120. Burgess, J., *Spectrochim. Acta A* **45,** 159 (1989).
121. Lewis, N. A., and Obeng, Y. S., *J. Am. Chem. Soc.* **111,** 7624 (1989).
122. Curtis, J. C., Sullivan, B. P., and Meyer, T. J., *Inorg. Chem.* **22,** 224 (1983).
123. Ennix, K. S., McMahon, P. T., de la Rosa, R., and Curtis, J. C., *Inorg. Chem.* **26,** 2660 (1987).
124. Curtis, J. C., Blackbourn, R. L., Ennix, K. S., Hu, S., Roberts, J. A., and Hupp, J. T., *Inorg. Chem.* **28,** 3791 (1989).
125. Curtis, J. C., Roberts, J. A., Blackbourn, R. L., Dong, Y., Massum, M., Johnson, C. S., and Hupp, J. T., *Inorg. Chem.* **30,** 3856 (1991).
126. Hupp, J. T., and Weydert, J., *Inorg. Chem.* **26,** 2657 (1987).
127. Todd, M. D., Dong, Y., and Hupp, J. T., *Inorg. Chem.* **30,** 4685 (1991).
128. Hupp, J. T., *J. Am. Chem. Soc.* **112,** 1563 (1990).
129. Hupp, J. T., Kober, E. M., Neyhart, G. A., and Meyer, T. J., *in* "Mixed-Valency Systems: Applications in Chemistry, Physics and Biology" (Prassides, K., Ed.), p. 51. Kluwer Academic, Dordrecht, 1991.
130. Dong, Y., and Hupp, J. T., *Inorg. Chem.* **31,** 3322 (1992).
131. Hupp, J. T., and Dong, Y., *J. Am. Chem. Soc.* **115,** 6428 (1993).
132. (a) Marcus, R. A., and Sutin, N., *Biochim. Biophys. Acta* **811,** 265 (1985); (b) Hush, N. S., *Coord. Chem. Rev.* **64,** 135 (1985).
133. (a) Joachim, C., Launay, J. P., and Woitellier, S., *Chem. Phys.* **147,** 131 (1990); (b) Launay, J. P., *in* "Mixed-Valency Systems: Applications in Chemistry, Physics and Biology" (Prassides, K., Ed.), p. 321. Kluwer Academic, Dordrecht, 1991.
134. Beratan, D. N., and Hopfield, J. J., *J. Am. Chem. Soc.* **106,** 1584 (1984).
135. Siddarth, P., and Marcus, R. A., *J. Phys. Chem.* **94,** 2985 (1990).
136. Isied, S. S., Vassilian, A., and Wishart, J. F., *J. Am. Chem. Soc.* **110,** 635 (1988).
137. Katz, N. E., Creutz, C., and Sutin, N., *Inorg. Chem.* **27,** 1687 (1988).
138. Gesolowitz, D. A., *Inorg. Chem.* **26,** 4135 (1987).
139. Hale, P. D., and Ratner, M. A., *Int. J. Quant. Chem.* **18,** 195 (1984).
140. Joachim, C., *Chem. Phys. Lett.* **185,** 569 (1991).
141. Hage, R., Haasnoot, J. G., Reedijk, J., and Vos, J. G., *Chemtracts* **4,** 75 (1992).
142. Curtis, J. C., Bernstein, J. S., Schmehl, R. H., and Meyer, T. J., *Chem. Phys. Lett.* **81,** 48 (1981).

143. Curtis, J. C., Bernstein, J. S., and Meyer, T. J., *Inorg. Chem.* **24,** 385 (1985).
144. Doon, S. K., Stoutland, P. O., Dyer, R. B., and Woodruff, W. H., *J. Am. Chem. Soc.* **114,** 3133 (1992).
145. Klinger, D. A. V., Tominaga, K., Walker, G. C., and Barbara, P. F., *J. Am. Chem. Soc.* **114,** 8323 (1992).
146. Doon, S. K., Dyer, R. B., Stoutland, P. O., and Woodruff, W. H., *J. Am. Chem. Soc.* **115,** 6398 (1993).
147. Joachim, C., and Launay, J. P., *Chem. Phys.* **109,** 93 (1986).
148. Woitellier, S., Launay, J. P., and Joachim, C., *Chem. Phys.* **131,** 481 (1989).
149. Marvaud, V., and Launay, J.-P., *Inorg. Chem.* **32,** 1376 (1993).
150. Hanack, M., Deger, S., and Lange, A., *Coord. Chem. Rev.* **83,** 135 (1988).
151. Kobel, W., and Hanack, M., *Inorg. Chem.* **25,** 103 (1986).
152. Keppeler, U., Deger, S., Lange, A., and Hanack, M., *Angew. Chem.* **99,** 349 (1987).
153. For example see (a) Petersen, J. D., *in* "Supramolecular Photochemistry" (Balzani, V., Ed.), p. 135. Reidel, Dordrecht, 1987; (b) Campagna, S., Denti, G., Serroni, S., Ciano, M., Juris, A., and Balzani, V., *Inorg. Chem.* **31,** 2982 (1992); (c) Arana, C. R., and Abruna, H. D., *Inorg. Chem.* **32,** 194 (1993); (d) Serroni, S., Denti, G., Campagna, S., Juris, A., Ciano, M., and Balzani, V., *Angew. Chem. Int. Ed. Engl.* **31,** 1493 (1992); and references cited therein.
154. Daudey, J. P., De Loth, P., and Malrieu, J. P., *in* "Magneto-Structural Correlations in Exchange Coupled Systems" (Willet, R. D., Gatteschi, D., and Kahn, O., Eds.), p. 87. Reidel, Dordrecht, 1985.
155. Anderson, P. W., *Phys. Rev.* **115,** 2 (1959).
156. Hopfield, J. J., *in* "Tunneling in Biological Systems" (Chance, B., De Vault, D. C., Frauenfelder, H., Marcus, R. A., Schrieffer, J. R., and Sutin, N., Eds.). Academic Press, New York, 1979.
157. Okamura, M. Y., Fredkin, D. R., Isaacson, R. A., and Feher, G., *in* "Tunneling in Biological Systems" (Chance, B., De Vault, D. C., Frauenfelder, H., Marcus, R. A., Schrieffer, J. R., and Sutin, N., Eds.), p. 729. Academic Press, New York, 1979.
158. Hay, P. J., Thibeault, J. C., and Hoffmann, R., *J. Am. Chem. Soc.* **97,** 4884 (1975).
159. Bertrand, P., *Chem. Phys. Lett.* **113,** 104 (1985).
160. (a) Kahn, O., and Briat, B., *J. Chem. Soc., Faraday II,* 268 (1976); 1441 (1976); (b) Kahn, O., *in* "Magneto-Structural Correlations in Exchange Coupled Systems" (Willet, R. D., Gatteschi, D., and Kahn, O., Eds.), p. 37. Reidel, Dordrecht, 1985.
161. Lever, A. B. P., "Inorganic Electronic Spectroscopy," 2nd ed., p. 220. Elsevier, Amsterdam, 1984.
162. Hale, P. D., Ratner, M. A., and Hofacker, G. L., *Chem. Phys. Lett.* **119,** 264 (1985).
163. Kramers, H. A., *Physica* **1,** 182 (1934).
164. Crutchley, R. J., McCaw, K., Lee, F. L., and Gabe, E. J., *Inorg. Chem.* **29,** 2576 (1990).
165. Saleh, A. A., and Crutchley, R. J., *Inorg. Chem.* **29,** 2132 (1990).
166. Crutchley, R. J., Saleh, A. A., McCaw, K., and Aquino, M. A. S., *Mol. Cryst. Liq. Cryst.* **194,** 93 (1991).
167. For a good introduction to magnetism, see Drago, R. S., "Physical Methods for Chemists," 2nd. ed. Chap. 11. Saunders, Orlando, 1992.
168. Carlin, R. L., "Magnetochemistry." Springer-Verlag, Berlin/Heidelberg, 1986.
169. Drillon, M., and Georges, R., *Phys. Rev. B* **24,** 1278 (1981).
170. Johnson, E. C., Callahan, R. W., Eckberg, R. P., Hatfield, W. E., and Meyer, T. J., *Inorg. Chem.* **18,** 618 (1979).
171. Bunker, B. C., Drago, R. S., Hendrickson, D. N., Richman, R. M., and Kessell, S. L., *J. Am. Chem. Soc.* **100,** 3805 (1978).

172. Figgis, B. N., *Prog. Inorg. Chem.* **6,** 173 (1964).
173. Hendrickson, D. N., *in* "Magneto-Structural Correlations in Exchange Coupled Systems" (Willet, R. D., Gatteschi, D., and Kahn, O., Eds.), p. 523. Reidel, Dordrecht, 1985.
174. Aquino, M. A. S., Lee, F. L., Gabe, E. J., Bensimon, C., and Crutchley, R. J., *Acta Crystallogr. C* **49,** 1543 (1993).
175. Aquino, M. A. S., Lee, F. L., Gabe, E. J., Bensimon, C., Greedan, J. E., and Crutchley, R. J., *Inorg. Chem.* **30,** 3234 (1991).
176. Naklicki, M. L., and Crutchley, R. J., submitted for publication.
177. Ondrechen, M. J., and Wu, X. M., *in* "Mixed-Valency Systems: Applications in Chemistry, Physics and Biology" (Prassides, K., Ed.), p. 335. Kluwer Academic, Dordrecht, 1991.
178. Ondrechen, M. J., Gozashti, S., Zhang, L.-T., and Zhou, F., *in* "Electron Transfer in Biology and the Solid State" (Johnson, M. K., King, R. B., Kurtz, D. M., Jr., Kutal, C., Norton, M. L., and Scott, R. A., Eds.), Chap. 12. American Chemical Society, Washington, D.C., 1990.